جامعة الإمارات العربية المتحدة
United Arab Emirates University

MASTER THESIS NO. 2022: 103

College of Engineering

Department of Electrical and Communication Engineering

NEURAL NETWORK BASED REACTIVE CONTROL OF POINT ABSORBER WAVE ENERGY CONVERTERS

Abdelmoamen Ali Nasser

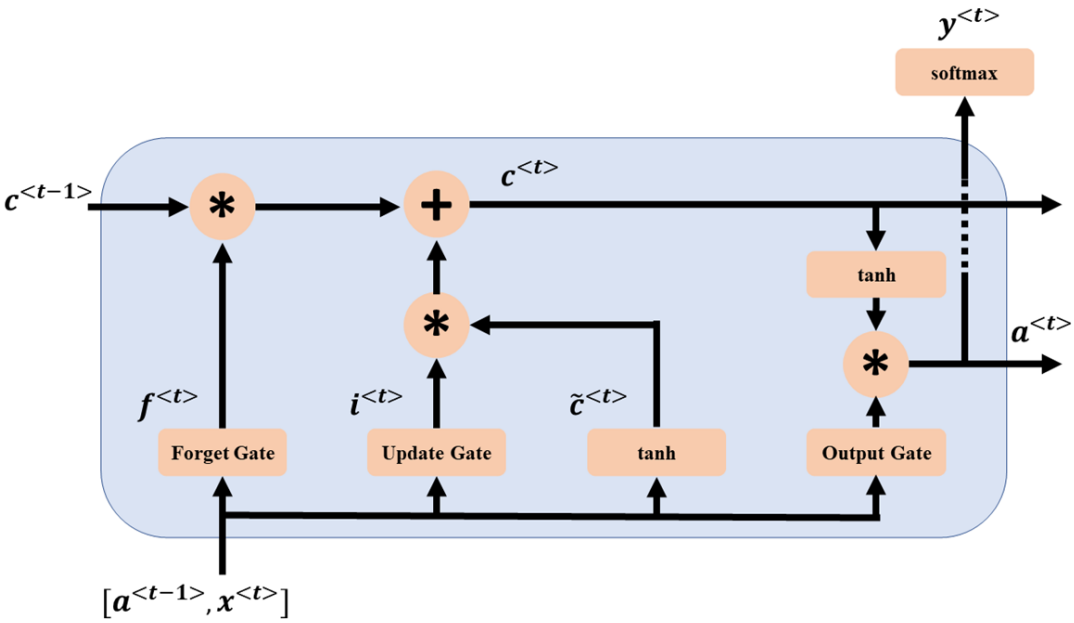

November 2022

United Arab Emirates University

College of Engineering

Department of Electrical and Communication Engineering

NEURAL NETWORK BASED REACTIVE CONTROL OF POINT ABOSRBER WAVE ENERGY CONVERTERS

Abdelmoamen Ali Nasser

This dissertation is submitted in partial fulfilment of the requirements for the degree of Master of Science in Electrical Engineering

November 2022

United Arab Emirates University Master Thesis
2022: 103

Cover: Long Short Term Memory Cell

(Diagram: By Abdelmoamen Ali Nasser)

Print: University Print Service, UAEU 2022

Declaration of Original Work

I, Abdelmoamen Ali Nasser, the undersigned, a graduate student at the United Arab Emirates University (UAEU), and the author of this thesis entitled "*Neural Network Based Reactive Control of Point Absorber Wave Energy Converters*", hereby, solemnly declare that this is the original research work done by me under the supervision of Dr. Addy Wahyudie in the College of Engineering at UAEU. This work has not previously formed the basis for the award of any academic degree, diploma or a similar title at this or any other university. Any materials borrowed from other sources (whether published or unpublished) and relied upon or included in my thesis have been properly cited and acknowledged in accordance with appropriate academic conventions. I further declare that there is no potential conflict of interest with respect to the research, data collection, authorship, presentation and/or publication of this thesis.

Student's Signature: 

Date: 22/12/2022

Approval of the Master Thesis

This Master Thesis is approved by the following Examining Committee Members:

1) Advisor (Committee Chair): Dr. Addy Wahyudie
   Title: Assistant Professor
   Department of Electrical Engineering
   College of Engineering
   Signature Addy Wahyudie Date 02/01/2023

2) Member: Dr. Qurban Ali Memon
   Title: Associate Professor
   Department of Electrical Engineering
   College of Engineering
   Signature Qurban Ali Date 02/01/2023

3) Member: Dr. Rachid Errousi
   Title: Assistant Professor
   Department of Electrical Engineering
   College of Engineering
   Signature Date 03/01/2022

4) Member: Prof. Xiao Xi (External Examiner)
   Title: Professor
   Department of Electrical Engineering
   Institute: Tsinghua University, China
   Signature Date 04/01/2023

This Master Thesis is accepted by:

Acting Dean of the College of Engineering: Professor Mohamad Al-Marzouqi

Signature Mohamed AlMarzouqi

Date February 09, 2023

Dean of the College of Graduate Studies: Professor Ali Al-Marzouqi

Signature Ali Hassan

Date 10/02/2023

Abstract

The main objective of this work is to develop a neural-network-based Reactive Control (RC) system for wave energy converters. The ability to maximize the power output of WEC while maintaining operation constraints, which can be physical or thermal, is crucial to the development of deployable control strategies. Having a control method that is robust, which means it handles uncertainty and noise very well, is one of the main performance criteria in evaluating the method. Therefore, this work starts by deriving an averaged WEC model to be simulated in MATLAB/Simulink. Additionally, the concepts of resistive loading control and reactive control (approximate conjugate control) are discussed. A solution to sea state estimation is developed and explained which poses a contribution the current WEC research. This novel technique uses recurrent neural networks (RNNs) with time-series data input to estimate the sea state in real-time. The technique fills the gap of estimating forces based on peak frequencies and also the problem of calculating sea states based on periodical averaged statistical analysis. To complete the methodology, an optimization technique using feed forward neural networks is improved to perform optimization that is proposed to optimize the power output with respect to the sea states. This is done by using the neural network as a cost function while using the physical limitations of the system as a constraint. The neural networks in this work are developed, trained and tested using MATLAB's Deep Network Designer and Deep Learning Toolbox then imported as a Simulink block to complete the simulation. The results are evaluated for each of the section. First, initial logging of the performance metrics, such as mean power, is done prior to the addition of any neural networks. The accuracy and robustness of the sea state estimation RNN is then discussed. Finally, a comparison between traditional reactive Control optimized and reactive Control is conducted. To summarize the outcome, after experimenting with different datasets and architectures, the RNN is able to estimate sea states in real-time under different initial conditions.

Keywords: Neural network, recurrent neural networks, reactive control, wave energy converters, deep learning, approximate conjugate control, sea state estimation.

Title and Abstract (in Arabic)

تطوير نظام التحكم التفاعلي (RC) القائم على الشبكة العصبية لمحولات طاقة الأمواج

الملخص

الهدف الرئيسي من هذا العمل هو تطوير نظام التحكم التفاعلي القائم على الشبكة العصبية لمحولات طاقة الأمواج .تعد القدرة على تعظيم إنتاج الطاقة من (WEC) مع الحفاظ على قيود التشغيل ، والتي يمكن أن تكون فيزيائية أو حرارية ، أمًرا بالغ الأهمية لتطوير استراتيجيات التحكم القابلة للنشر. يعد وجود طريقة تحكم قوية ، مما يعني أنها تتعامل مع عدم اليقين والضوضاء جيدًا ، أحد معايير الأداء الرئيسية في تقييم الطريقة. لذلك ، يبدأ هذا العمل باشتقاق نموذج (WEC) متوسط ليتم محاكاته في سيميولينك و ماتلاب بالإضافة إلى ذلك ، تمت مناقشة مفاهيم التحكم في التحميل المقاوم والتحكم التفاعلي (التحكم المتقارن التقريبي). تم تطوير وشرح حل لتقدير حالة البحر مما يشكل مساهمة في أبحاث (WEC) الحالية. تستخدم هذه التقنية الجديدة الشبكات العصبية المتكررة مع إدخال بيانات السلاسل الزمنية لتقدير البحر في الوقت الفعلي. تملأ هذه التقنية فجوة تقدير القوى بناًء على تردد حالات الذروة وأيًضا مشكلة حساب حالات البحر بناًء على التحليل الإحصائي الدوري المتوسط. لإكمال المنهجية ، تم تحسين تقنية التحسين باستخدام الشبكات العصبية (Feed Forward) لأداء التحسين المقترح لتحسين خرج الطاقة فيما يتعلق بحالات البحر. يتم ذلك باستخدام الشبكة العصبية كدالة تكلفة أثناء استخدام القيود المادية للنظام كقيد. تم تطوير الشبكات العصبية في هذا العمل وتدريبها واختبارها باستخدام مصمم الشبكات العصبية العميقة ثم استخراجها ككتلة (Simulink) لإكمال المحاكاة. يتم تقييم النتائج لكل قسم. أولاً ، يتم التسجيل الأولي لمقاييس الأداء ، مثل متوسط القوة ، قبل إضافة أي شبكات عصبية. ثم تتم مناقشة دقة ومتانة تقدير حالة البحر بالشبكة العصبية المتكررة. أخيرا ، تم إجراء مقارنة بين التحكم التفاعلي التقليدي المحسن للتحكم التفاعلي. لتلخيص النتيجة ، بعد تجربة مجموعات البيانات والبنى المختلفة ، تستطيع بالشبكة العصبية المتكررة تقدير الحالات البحرية في الوقت الفعلي في ظل ظروف أولية مختلفة.

مفاهيم البحث الرئيسية: الشبكة العصبية، الشبكات العصبية المتكررة، التحكم التفاعلي، محولات طاقة الأمواج، التحكم المقترن التقريبي، تقدير حالة البحر، التعلم العميق.

Author Profile

Abdelmoamen Ali Nasser is currently an Artificial Intelligence Intern at the Lockheed Martin Center for Innovation & Security Solutions located at Masdar City, Abu Dhabi, UAE where he gained experience in deep learning and their applications to industry specific projects. Abdelmoamen was in the winning team at the "Youth Hackathon on the Energy Sector in the UAE" organized by the French Institute, Total Energies CEO Mr. Elias Kassis and the French Ambassador in the UAE H.E Xavier Chatel. Abdelmoamen received his BSc. in Electrical Engineering degree from Abu Dhabi University in the UAE with a focus in power systems and renewable energy. He has published his under graduate thesis work titled "Viability Study of Photovoltaic Modules Floating on Water Lakes in Abu Dhabi" in the 2018 Energy Systems conference. His research interests are steering towards Intelligent Control with a new interest in robot autonomy.

Acknowledgements

First of all, All praise to Allah the Almighty for blessing me during my years of study and research.

Secondly, my deepest gratitude goes to my thesis supervisor Dr. Addy Wahyudie for his continuous guidance since the beginning. He steered me towards all the resources needed to conduct my research, write my thesis and answer all my questions. Without his guidance, this work would not have been complete and I'm very grateful to him. I would like to also extend my thanks to Dr. Addy's research team and the faculty members of the Department of Electrical and Communication Engineering for their support in providing resources.

Additionally, I would like to thank my co-workers for being a part of my growth as an engineer and a researcher. Being in such an encouraging environment facilitated this growth.

Finally, I would like to take this opportunity to thank my parents (Dr. Ali Tafour and Mrs. Manal Moustafa) and my siblings for their continuous support and understanding.

Dedication

To my great parents and beloved family

Table of Contents

Title i
Declaration of Original Work iii
Approval of the Master Thesis iv
Abstract vi
Title and Abstract (in Arabic) vii
Author Profile viii
Acknowledgements ix
Dedication x
Table of Contents xi
List of Tables xiii
List of Figures xiv
List of Abbreviations xvi
Chapter 1: Introduction 1
1.1 Importance of Harvesting Wave Energy 1
1.1.1 Fossil Fuel Consumption 1
1.1.2 Renewable Energy & Wave Energy 2
1.2 Characteristics of Waves & Wave Resource 2
1.3 Wave Energy Converters 3
1.4 Artificial Intelligence, neural networks and deep learning 4
1.5 Literature Review 6
1.6 Research Problem & Objectives 6
1.7 Structure of the Thesis 8
Chapter 2: Methodology 9
2.1 WEC Model 9
2.1.1 Excitation Force 10
2.1.2 Hydrostatic Buoyancy Force 13
2.1.3 Restoring Force 14
2.1.4 Drag Force 15
2.1.5 End-stop Force 15
2.1.6 Friction Force 15
2.1.7 Radiation Force 15

2.1.8 Electromagnetic force 18
2.1.9 Section Summary 22
2.2 Machine Side Converter Controller & PMLG System 22
2.2.1 Machine Side Converter Controller 23
2.2.2 PMLG System 25
2.3 Analysis Block 26
2.4 Sea state estimation using Recurrent Neural Networks 27
2.4.1 Data Collection 28
2.4.2 Recurrent Neural Network Architecture 30
2.5 Reactive Control using Neural Networks 34
Chapter 3: Results and Discussion 45
3.1 Simulation Environment 45
3.2 Simulation Results 46
3.2.1 Reactive control using neural networks 46
3.2.2 Sea state estimation using recurrent neural networks 48
Chapter 4: Conclusion 56
4.1 Research Findings & Summary 56
4.2 Limitations 56
4.3 Future Work 57
References 58

List of Tables

Table 1: Simulation Parameters 45
Table 2: Simulation Runtimes 46
Table 3: Sea States 46
Table 4: Optimized damping coefficients $\times 10^5$ 46
Table 5: Optimized stiffness coefficients $\times -10^5$ 47
Table 6: Traditional vs Optimized Reactive Control Outputs. Power $\times 10^4$ (W), Displacement (m). 47

List of Figures

Figure 1: Global Fossil Fuel Consumption 1
Figure 2: Wave Trough & Crest 3
Figure 3: Artificial Intelligence, Machine Learning & Deep Learning 5
Figure 4: Heaving WEC structure 8
Figure 5: Kex Magnitude and Phase 11
Figure 6: Pole-zero map for the excitation impulse response function of the cylindrical buoy 12
Figure 7: WAMIT generated data for the radiation resistance and radiation added mass in frequency domain 17
Figure 8: Pole-zero map for the cylindrical buoy 18
Figure 9: The magnitude and phase angle of the radiation frequency response function for the cylindrical buoy 18
Figure 10: Direct drive principle 19
Figure 11: Simulink block for the MSCC 24
Figure 12: Simulink block for the PMLG System 25
Figure 13: Half-Wave Height described in irregular waves 27
Figure 14: Data Collection Block for datasets including maximum buoy displacement as output 29
Figure 15: I/O diagram of LSTM Neuron 31
Figure 16: I/O diagram of GRU Neuron 33
Figure 17: Simulink block of RNN deployment 34
Figure 18: Feed forward NN architecture for the optimization algorithm as described by the original paper 35
Figure 19: Implementation used in this work of the network in Figure 18 35
Figure 20: Flow chart of the ANN training and data collection 37
Figure 21: Simulink Block of reactive control using look up tables 39
Figure 22: Fully neural network based controller 39
Figure 23: Simulink block for the WEC model 40
Figure 24: Simulink block for Resistive Loading 41
Figure 25: Simulink block for Reactive Control 42
Figure 26: Chosen RNN Architecture 43
Figure 27: Fully neural network based controller-Simulink 44
Figure 28: Mechanical power, electrical power and efficiency for a regular sea state of H_{hw} =3 m & T_{hw} =10 s. a) Traditional reactive control b) Optimized reactive control 48
Figure 29: Training graph for LSTM 50
Figure 30: Training progress graphs for RNNs 51
Figure 31: Prediction results for half wave height 52
Figure 32: Prediction results for half wave period 53

Figure 33: Prediction results for irregular waves 54
Figure 34: Prediction results for sequence of regular waves..... 55

List of Abbreviations

at	Activation output
ANN	Artificial Neural Network
$H_{1/3}$	Average height of one third of the waves
m_∞	Body added mass at infinite frequency
C_b	Buoyancy stiffness coefficient
C_D	Drag coefficient
f_d	Drag force
E_e	Electrical energy
E_m	Electromagnetic energy
f_u	Electromagnetic/control force
fes	End-stop force
$S(\omega)$	Energy spectrum
fex	Excitation Force
ψpm	Flux linkage amplitude
Γ_f	Forget gate
R_c	Frequency dependent resistance
f_f	Friction force
GAN	Generative Adversarial Network
GRU	Gradient Recurrent Unit
g	Gravitational acceleration
Hhw	Half-wave height
Thw	Half-wave period
f_b	Hydrostatic buoyancy force

P_e	Instantaneous electrical power
P_m	Instantaneous electromagnetic power
LSTM	Long Short Term Memory
p_w	Machine pole pitch
ct	Memory cell
Γ_o	Output gate
λpm	Permanent magnet flux
PMLG	Permanent magnet linear generator
$\eta pmlg$	PMLG efficiency
$fpto$	Power take-off force
PTO	Power take-off mechanism
M_r	Radiation added mass
R_r	Radiation resistance
RNN	Recurrent Neural Network
RL	Resistive loading
frs	Restoring force
S_r	Restoring Spring Coefficient
T_s	Sampling time
$Rpto$	Spring damping coefficient
$Kpto$	Spring stiffness coefficient
L_s	Stator inductance
R_s	Stator resistance
$Zint$	System intrinsic impedance
$Xint$	System intrinsic reactance
Γ_u	Update gate

$Vwater$	Volume of displaced water
ρ	Water density
A_w	Water plane area of the buoy
WEC	Wave Energy Converter
ω_p	Wave peak frequency
T_e	Wave peak period
H_s	Wave significant height
J	Wave transport

Chapter 1: Introduction

1.1 Importance of Harvesting Wave Energy

1.1.1 Fossil Fuel Consumption

As humanity progresses forward, having renewable resources of energy is crucial to the future of civilization since conventional energy generation methods will deplete the natural resources eventually. Since the start of the Industrial Revolution, the consumption of fossil fuels as a source of electricity globally has been increasing exponentially. As seen in Figure 1, the consumption went from 0 TWh in 1800 to more than 120,000 TWh in 2019 cumulatively (Coal, Gas and Oil) [1]. The data in the chart is a combination of statistics from [1] and data published in [2]. Currently, fossil fuel is the major source of energy use, responsible for 82% of global energy consumption. However, this is slowly changing since it was responsible for 85% of consumption five years ago. Needless to say, this high usage of fossil fuel is responsible for carbon emissions which contribute directly to environmental and health problems. According to the Intergovernmental Panel on Climate Change (IPCC), fossil fuel emissions are mainly responsible for global warming with 89% of the global CO_2 emissions. It is definitely a wise decision to diversify electricity generation sources since different studies predict the depletion of fossil fuel within the current century. The UAE has taken steps towards this diversification under the name of "UAE Energy Strategy 2050" [3].

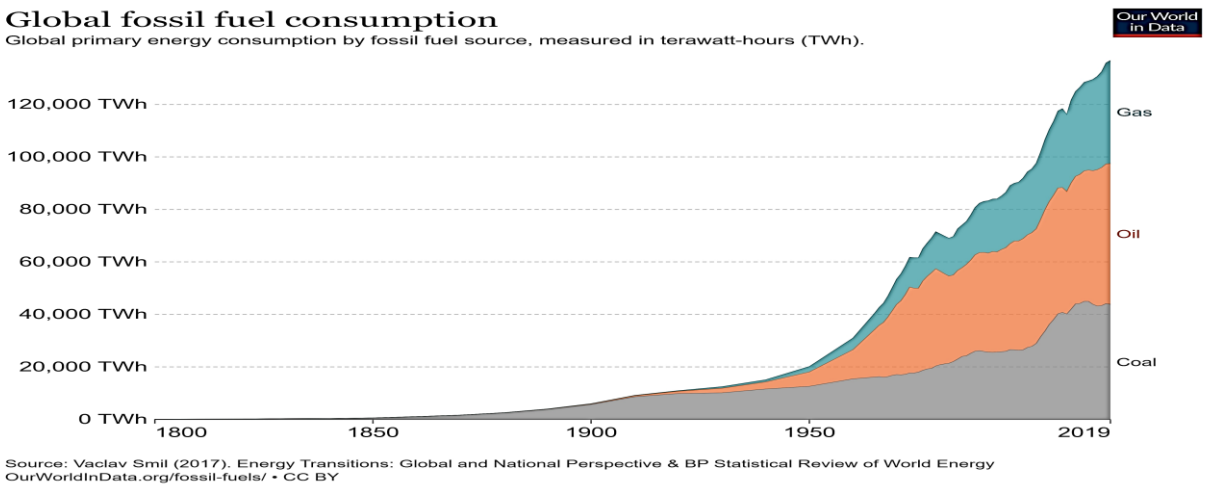

Figure 1: Global Fossil Fuel Consumption [4]

1.1.2 Renewable Energy & Wave Energy

According to the Center for Climate and Energy Solutions (C2ES), renewable energy has grown by 42% between the years 2010 and 2022, and 90% between the years 2000 and 2020 in the United States. This makes renewable energy the fastest growing energy resource in the United States [5]. More statistics from the C2ES highlight the role of hydro-power when contributing to the statistics regarding renewable energy. For example, in 2020, hydro power was responsible was responsible for 7.3% of electricity generation in the United States and 16.8% globally. That implies a huge room for improvement since the U.S. Energy Information Administration (EIA) has estimated the potential energy of waves in the United States to be around 2.64 trillion kWH, which covers 64% utility scale electricity generation. Even though wave energy has the potential of producing up to 2.1 TW globally. That can cover the global consumption of electricity. However, only a 25% of that is being harvested due to difficulties in harnessing that potential [6].

1.2 Characteristics of Waves & Wave Resource

Wave energy harvesting requires proper understanding of the characteristics that describe the energy content in the wave. This convention is used in ocean engineering based on statistical metrics. First of all, the source of energy content at the sea is fully dependent on the winds responsible for creating waves. While the winds have their own characteristics, the waves created also possess characteristics that describe the wave and its energy content. The first one of these characteristics is the significant height of the wave H_s, measured in m, which represents, for a regular or monochromatic wave, the distance between trough to crest of the wave. For irregular or poly-chromatic waves, this represents the average height of one third of the waves denoted as $H_{1/3}$ [7]. The other characteristic is the wave peak period T_e or peak frequency ω_p. This described the propagation speed of the wave [10]. The equations for the wave transport J, measured in kW/m for both kinds of waves respectively is related to both of the characteristics [8][9]. This is described as:

$$J = \frac{\rho g^2}{32\pi} T_e H_s^2 \tag{1.1}$$

where ρ is the water density (kg/m^3), g is gravitational acceleration (m/s^2):

$$J = \frac{\rho g^2}{2} \int_0^\infty \frac{S(\omega)}{\omega} \, \mathrm{d}\omega \tag{1.2}$$

where S(ω) is the energy spectrum. This signifies the importance of knowing these characteristics in terms of energy output.

To clearly define the difference between mono-chromatic and poly-chromatic waves, mono-chromatic (regular) waves consist of one wave component of the T_e and H_s. On the other hand, poly-chromatic waves are waves consisting of more than one component where they interfere, either destructively or constructively, to form a new wave of its own significant height and peak period.

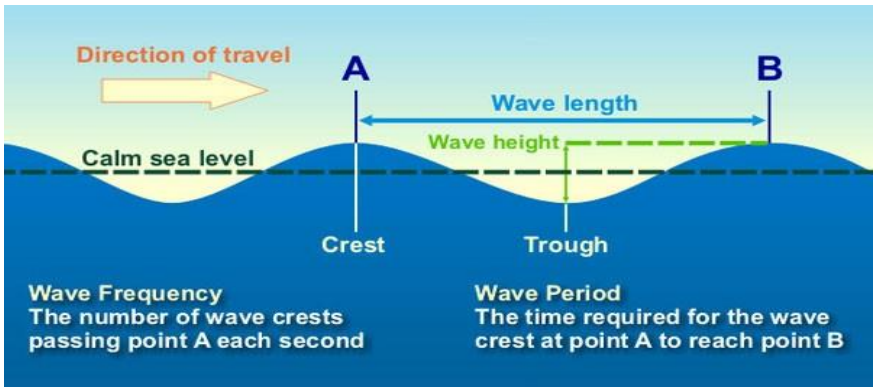

Figure 2: Wave Trough & Crest [10]

1.3 Wave Energy Converters

Similar to solar panels that capture solar energy, or wind turbines that capture wind energy, wave energy is harvested using devices called Wave Energy Converters (WECs). Generally, all WECs use the movement of waves to drive a generator. However, key differences in location, degree of freedom of motion, power take-off (PTO) mechanism and point of reaction classify them into different types [6]. For example, the type of wave energy converter discussed in this work, based on degree of freedom and PTO mechanism, is a heaving direct-drive point absorber WEC. In this type of WEC, the floating body usually referred to as the buoy is directly tethered to a Permanent Magnet Linear Generator (PMLG) which induces current whenever the waves cause the buoy to move.

In order to achieve maximum power absorption, resonance is required between the waves and the movement of the device. Therefore, Reactive Control (RC) can be used to achieve that objective, which by definition is the change in control signals in reaction to the system dynamics. In this case, this would be the change in control signal based on the velocity and displacement of the buoy. More details on these techniques are discussed in Chapter 2. The specific force that uses the RC model is the electromagnetic force, which is dependent on the damping and stiffness coefficients of the restoring springs of the system.

1.4 Artificial Intelligence, neural networks and deep learning

Artificial intelligence (AI) is a vast field that includes a lot of subsets that cover topics such as logic, probability, perception, learning and much more [11]. To put it simply, any attempt to mimic a human aspect of thinking by using machines can be referred to as artificial intelligence whether it is through hard coding statement or even complex algorithms. The origins of artificial intelligence can go back to 384 BCE when Aristotle formulated a precise set of laws governing the rational part of the mind. That was developed through the times by Ramon Llul’s "The Great Art", Da Vinci’s first mechanical calculator, Wilhelm Schickard’s and more scientists/inventors [11]. Machine learning is a subset of artificial intelligence and in turn, deep learning is a subset of machine learning. That is depicted by Figure 3.

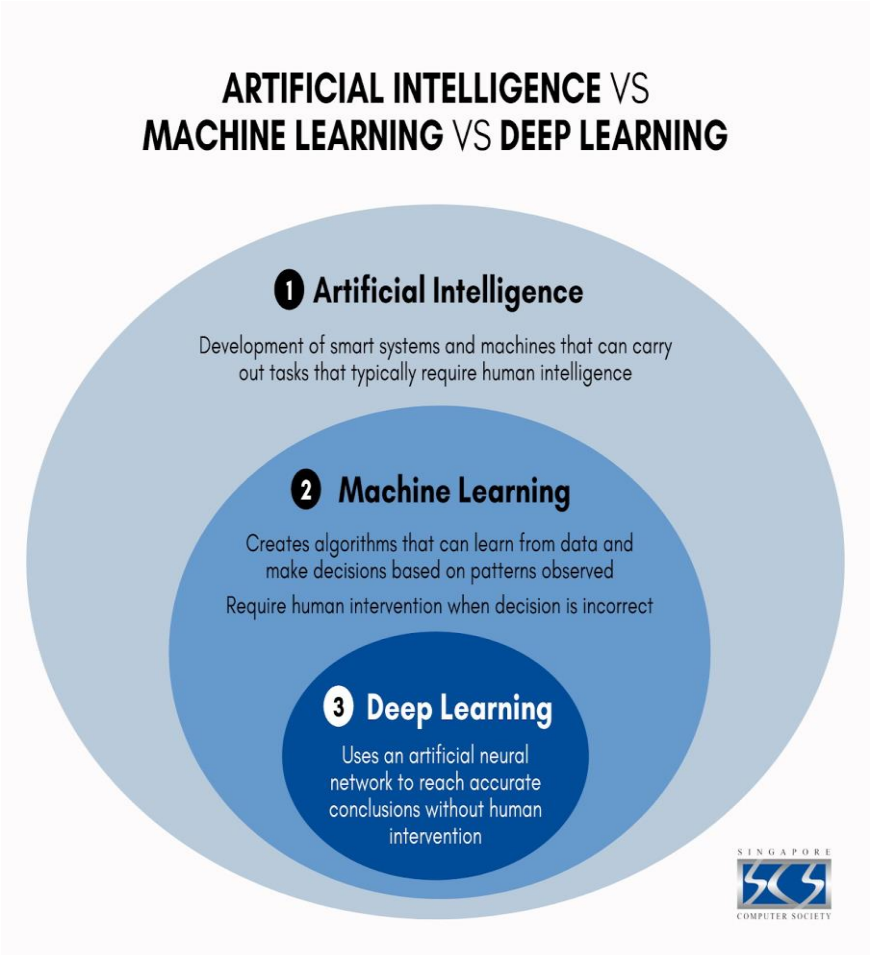

Figure 3: Artificial Intelligence, Machine Learning & Deep Learning [12]

A good starting point to trace back deep learning and specifically neural network is the McCulloch Pitts description of a neuron in their paper "A Logical Calculus Of The Ideas Immanent In Nervous Activity" [13]. This paper mathematically described neural events. Today, neural networks can be generally classified into three main classes based on inputs, outputs and applications. Feed forward neural networks or artificial neural networks (ANN), convolutional neural networks (CNN) and recurrent neural networks (RNN). The types used in this work are ANN and RNN. The vast increase in research in all of these types can be directly resorted to three main factors. The availability of datasets contributed directly to the progression of this field. Databases like Kaggle [14]. for example offer a variety of datasets that researchers can use to train their models. Furthermore, a class of neural networks called Generative Adversarial Networks (GAN) can be used to generate data [15]. The second reason is more computing power which allows models to be trained faster. An example for that is GPU accelerated training.

1.5 Literature Review

Research and Development of methods that optimize power absorption of wave energy converters is expanding. Traditional reactive control depends heavily on the power take off force which depends on knowledge of the current sea state. Artificial neural networks were used with an exploration based minimization algorithm to find optimal damping and stiffness coefficients while remaining within operation constraints of the wave energy converters [16].

However, this paper assumes a real time measurement of the current sea state. Other research used reinforcement learning, which is based on reward and penalty, for resistive and reactive control [17][18]. This type of work suffers from fluctuations in the prediction output of the neural network model. Non neural network based methods that were published recently use optimization to maximize power absorption while constraining the power flow in the positive direction, meaning the device never operates as a motor [19]. As mentioned earlier, most methods require information on the sea state, and that area has been explored by researchers. One paper was able to use artificial neural networks to predict displacement based on the most recent 60 seconds of observed data in H_s and T_e [20]. Another paper used an electrical extended kalman filter to estimate displacement values and calculate excitation force based on current measurements, which eliminates the need for mechanical sensors and exchanges it with the less expensive, more durable current transducers [21].

The biggest point of improvement that can be added to these methods is real-time, shorter period sea state estimation. More improvements can be explored in long term deployment, where degradation of performance due to rust or growth of marine life on the device can affect the performance. Finally, all these methods assume the statistical definition of significant height and wave frequency rather than dealing with waves on a peak to crest basis.

1.6 Research Problem & Objectives

To enhance power absorption in wave energy converters, machine resonance with the sea state must be achieved. This is directly related to careful choice of damping and stiffness coefficients of the restoring springs of the system. Therefore, optimized reactive

control should be used to maximize power absorbing while remaining in the operational constraints of the machine. The final piece that makes all the mentioned aspects possible is knowledge of the current sea state. Based on the previous statement, this thesis aims to:

- Use state of the art research to improve reactive control power harvesting using neural networks.
- Estimate the current sea state in real-time over shorter periods.
- Build a neural network based controller that utilizes sea state info and optimal coefficients for reactive control.

The following objectives are implemented on a heaving point absorber WEC that consists of a single body seabed reacting wave energy converters. The main components of this WEC are a permanent magnet linear generator (PMLG), tether and buoy. The heave movement of the buoy directly moves the permanent magnet to induce electricity. The structure of this WEC can be shown in Figure 4.

The scope of this work is mainly focused on:

- Machine side, therefore implementation of bi-directional power control is not considered.
- This work is non-experimental. All the acquired results are simulation based.
- It is assumed that a measurement of displacement is available, therefore methods for estimating or measuring displacement are not developed.

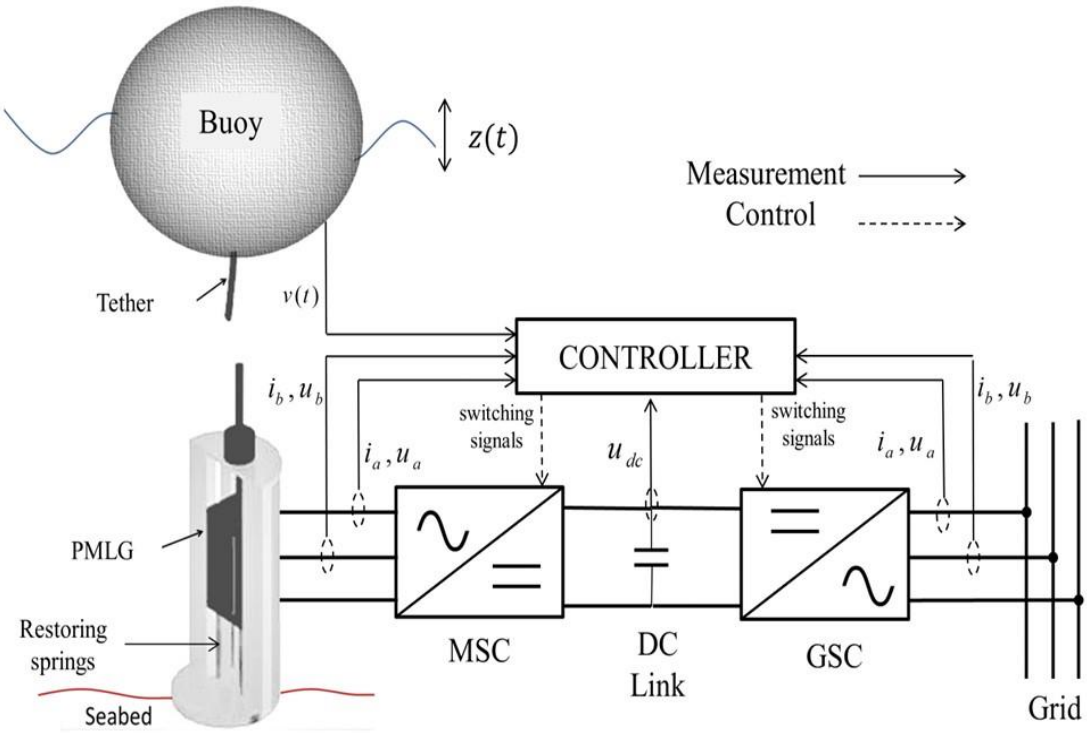

Figure 4: Heaving WEC structure [22]

1.7 Structure of the Thesis

This work is divided into 4 main chapters. Chapter 2 is the methodology section describing all the equations, derivation, models and implementation of the WEC control technique, analysis and neural networks. Chapter 3 goes over the results and the testing criteria for evaluation. Additionally, it discusses the logic and/or intuition behind these results. Finally, Chapter 4 summarizes the results and findings of this work while discussing future work and recommendations of the author.

Chapter 2: Methodology

In this chapter, all the equations, formulas, state-space models are explained in the first section. These equations and derivations are used with MATLAB & Simulink to simulate the operation of the WEC under different pre-generated sea state conditions. The second section will discuss the improvement of power absorption by including copper losses in the control blocks of the model [23]. The third section will go into the use of ANNs to optimize power absorption of the system while maintaining the operational constraints [16]. Finally, the fourth section will detail the novel real-time sea state estimation techniques developed by the use of RNNs.

2.1 WEC Model

The model described in this section is simulated in MATLAB & Simulink using time domain models of the forces affecting the WEC [22]. According to Newton's second law, all the forces affecting the system consisting of the buoy and PMLG translator can be described as follows:

$$f_{ex}(t) + f_u(t) - f_b(t) - f_{rs}(t) - f_d(t) - f_{es}(t) - f_f(t) - f_r(t) = ma(t) \qquad (2.1)$$

These forces are listed respectively and the modeling of each one of these forces will be discussed:

- Excitation force.
- Hydrostatic buoyancy force.
- Restoring force.
- Drag force.
- End-stop force.
- Friction force.
- Radiation force.
- Electromagnetic force which is also referred to as the control force.

2.1.1 Excitation Force

The excitation force is the sum of hydrodynamic pressure applied to the buoy by the incident waves [22][24]. The excitation force in time domain can be represented by the following integral [22]:

$$f_{ex}(t) = \int_{-\infty}^{\infty} k_{ex}(\tau - t)\eta(\tau)\, d\tau \tag{2.2}$$

where $k_{ex}(t)$ is the excitation impulse response function and $\eta(t)$ is the undistributed wave elevation. The fourier transform of the excitation force can be written as [22]:

$$F_{ex}(i\omega) = \mathcal{F}\big(f_{ex}(t)\big) = \int_{-\infty}^{\infty} e^{j\omega t} f_{ex}(t)\, dt \tag{2.3}$$

and to find the frequency domain equation of the excitation force, Fourier transform can be applied to Equation 2.2 [22]:

$$F_{ex}(i\omega) = K_{ex}(i\omega)H(i\omega) \tag{2.4}$$

where $H(i\omega)$ is the Fourier transform of the wave elevation and K_{ex} is the excitation force coefficient in the frequency domain. For a cylindrical buoy, semi-submerged, with a radius of 2.5 m and a draft of 1.5 m, WAMIT was used to obtain magnitude and phase values of wave elevation and excitation coefficient in frequency domain for a range of frequencies. WAMIT sets the wave elevation Fourier transform to 1 which makes the excitation force in frequency domain equal to the excitation coefficient. This data is plotted in Figure 5.

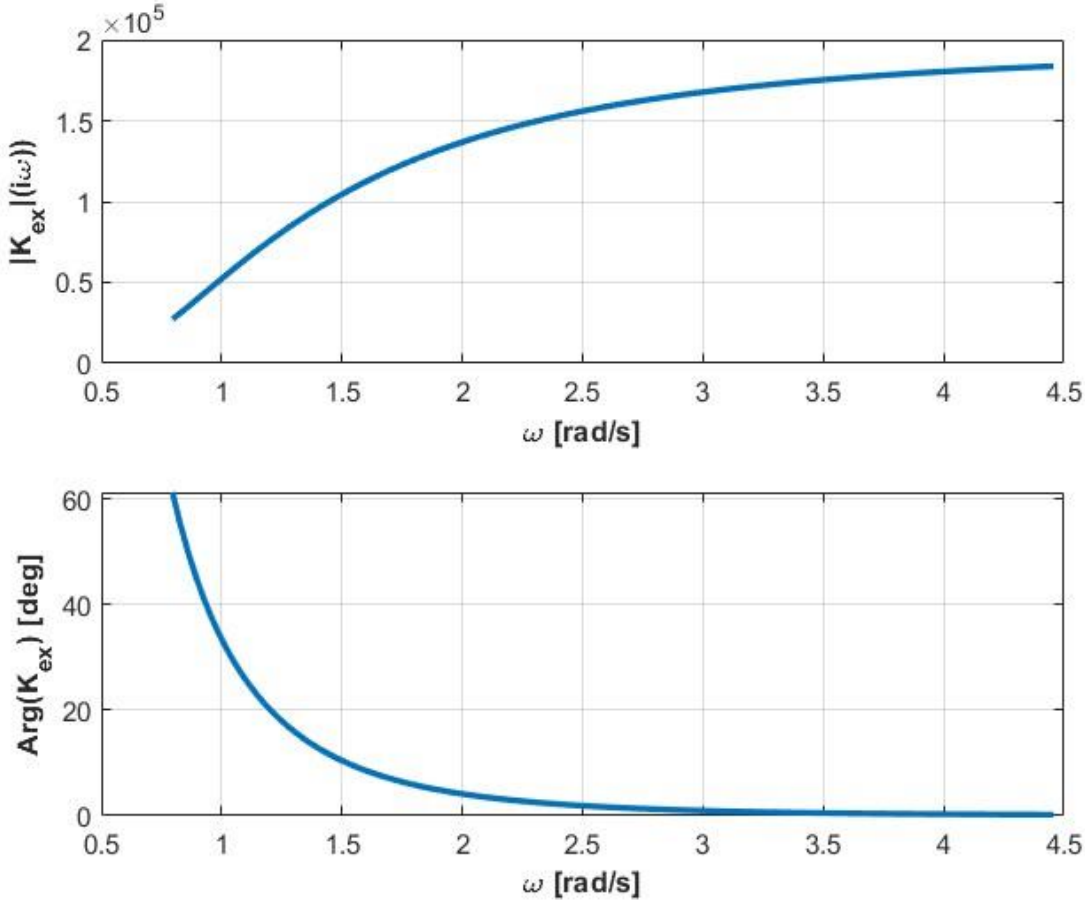

Figure 5: Kex Magnitude and Phase

However, the excitation force is non-causal [8]. Therefore, a small time delay is introduced, and the causal counterpart is [26]:

$$\widehat{K}_{ex}(i\omega) = K_{ex}(i\omega)e^{-i\omega\tau} \tag{2.5}$$

$\widehat{K}_{ex}(i\omega)$ is causal and τ is the introduced small time delay. A frequency based technique is used to utilize the WAMIT generated data and approximate a transfer function [25] as follows:

$$\hat{K}_{ex}(i\omega) \approx \frac{N(i\omega)}{D(i\omega)} \approx \frac{b_m(i\omega)^m + b_{m-1}(i\omega)^{m-1} + ... + b_0}{a_n(i\omega)^n + a_{n-1}(i\omega)^{n-1} + ... + a_0} \tag{2.6}$$

This is a polynomial where the numerator is of the m-th order and the denominator is of the n-th order. To express this in LaPlace domain, we simply replace iω by s:

$$\hat{K}_{ex}(s) \approx \frac{N(s)}{D(s} \approx \frac{b_m(s)^m + b_{m-1}(s)^{m-1} + ... + b_0}{a_n(s)^n + a_{n-1}(s)^{n-1} + ... + a_0} \tag{2.7}$$

The order n has to be found using iterative methods to ensure that $\widehat{K}_{ex}(s)$ is strictly proper [27]. This order n is dependent on the hydrodynamics of the cylindrical body which also depends in its geometry. MATLAB is used with the function "invfreqs" to compute the coefficients [22]. This is called the Least-squares based method. Unstable poles were produced as a result of this method, however they were simply reflected to the left hand side to stabilize them [27]. This is due to the stability property of linear time invariant systems where all the poles (roots of denominator) need to have a negative real part. The approximated $\widehat{K}_{ex}(s)$ is:

$$\hat{K}_{ex}(s) \approx 1 \times 10^5 \frac{0.3711s^{10} + 0.8216s^9 + 3.549s^8 + 5.935s^7}{s^{10} + 1.046s^9 + 7.279s^8 + 6.233s^7 + 18.81s^6} \frac{+11.82s^6 + 14.8s^5 + 16.24s^4 + 14.65s^3 + 7.712s^2 + 4.537s}{+12.4s^5 + 20.21s^4 + 9.093s^3 + 7.566s^2 + 1.631s + 0.1271} \tag{2.8}$$

and the pole-zero map for this function is shown in Figure 6 where it can be observed clearly that it is stable:

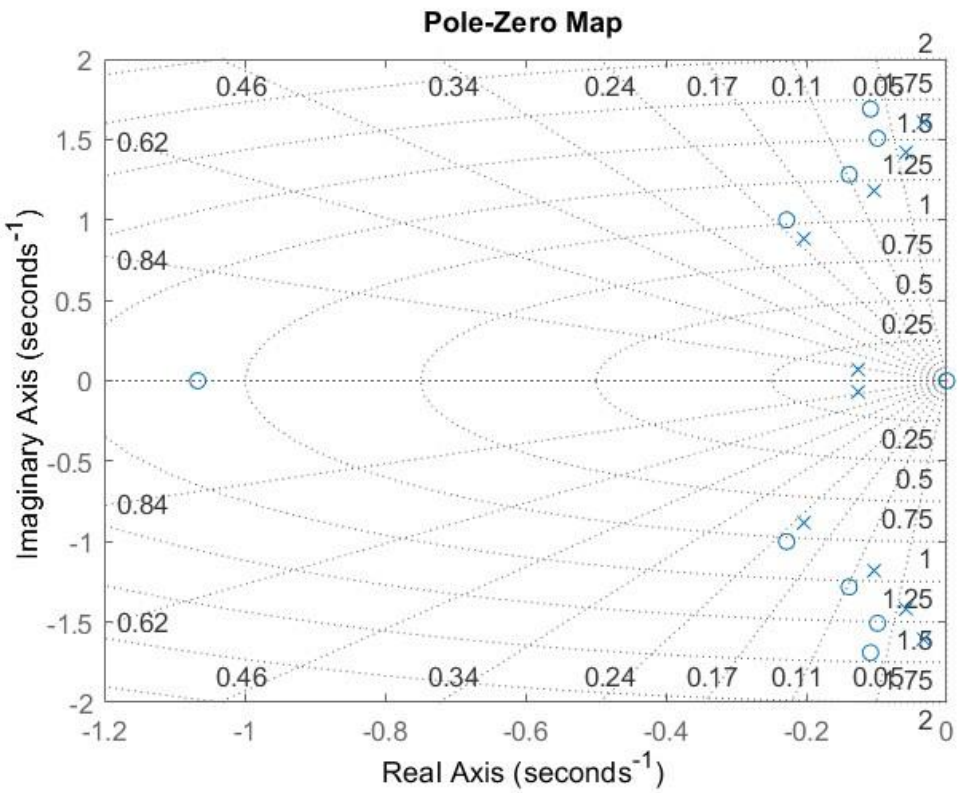

Figure 6: Pole-zero map for the excitation impulse response function of the cylindrical buoy

The numerator and denominator coefficients can be used as input to the function "tf2ss" to find the state space matrices of the excitation force which will be used in the Simulink model to represent the excitation force.

As mentioned in [8], the system is able to absorb the maximum power when the excitation force is in phase with the heave velocity which is referred to as "resonance". Resonance is achieved when the natural frequency of the system is equal to the dominant frequency of the wave causing motion [28]. The natural frequency is the frequency that the body will be oscillating at if excited and left to heave freely with no driving force [29]. Since the dynamics of the system is dominated by its intrinsic impedance when heaving freely, the reference velocity of maximum power absorption is [22]:

$$v^* = \frac{\tilde{f}_{ex}(t)}{2R_{int}(\omega)} cos(\phi) \tag{2.9}$$

where $\tilde{f}_{ex}$ is the reference/estimated excitation force, $R_{int}(\omega)$is the intrinsic resistance and ϕ is the phase difference between the actual velocity and estimated excitation force. However, a short coming of this expression is the noncausality of the excitation force and the need for a real time wave frequency determination. A solution for the second drawback will be discussed later on in this work.

2.1.2 Hydrostatic Buoyancy Force

Hydrostatic Buoyancy Force $f_b(t)$ is the force generated due to the variation of hydro-static pressure whenever the floating body moves [22]. The mathematical representation of this force stems from the difference between the weight of the moving buoy and the weight of displaced water, the water that is displaced by the movement of the body. This is due to the fact that in equilibrium these two terms are equal, but they are mismatched when the body is in motion [8][22]:

$$f_b(t) = mg - \rho g V_{water} \tag{2.10}$$

where m is the mass of the buoy, g is gravitational acceleration, ρ is density of water and V_{water} is water volume that has been displaced. Hydro-static buoyancy force is proportional to the current displacement of the body from equilibrium. However, it is opposite to it in direction:

$$f_b(t) = -C_b z(t) \tag{2.11}$$

where C_b is the buoyancy stiffness coefficient expressed as:

$$C_b = \rho g A_w \tag{2.12}$$

A_w is the water plan area of the floating body. In other words, it is the area of a cross section of the floating the body that is in line with the water surface. For a cylindrical body, this can be measured as:

$$A_w = \pi r^2 \tag{2.13}$$

where r is the radius of the buoy. In the context of this thesis, the radius is 2.5 m. This is easily modeled in Simulink by substituting the radius in the equations to find the coefficient and modeling the force as mentioned in Equation 2.11.

2.1.3 Restoring Force

The restoring force $f_{rs}(t)$ is the force resulting from the springs between the linear translator of the PMLG and the seabed [30]. The springs serve two main functions:

- Support gravity in bringing down the buoy to equilibrium after upward motion (wave crest).
- Pull the slack out of the tether, ensuring its always stretched. This eliminates the effects accompanied by a loose tether [31].

The mathematical representation of the restoring force is very similar to the hydro-static buoyancy force. In this case the coefficient multiplied by the displacement is the restoring spring coefficient:

$$f_{rs} = -S_r z(t) \tag{2.14}$$

Once again, this is easily modeled in Simulink based on prior knowledge of the restoring spring coefficient $S_r = 6 \times 10^4$

2.1.4 Drag Force

Drag force $f_d(t)$is a result of the force applied by sea waves to the buoy in the direction of their travel. Morison's equation has always been used to describe these phenomena [32][33]. The full expression consists of two terms. However, only the drag term is considered in this thesis:

$$f_d(t) = 0.5\rho A_w C_D v(t)|v(t)| \tag{2.15}$$

Where the drag coefficient C_D can be determined experimentally based on flow conditions and Reynolds number [34].

2.1.5 End-stop Force

In addition to the bottom springs responsible the restoring force, another set of springs are placed at the upper side of the PMLG enclosure to prevent it from hitting the enclosure aggressively as it experiments fast wave periods or large significant heights. This makes them active at the top of the wave crest where the translator is maximally displaced [35]. This force is not modeled in this work.

2.1.6 Friction Force

Friction force is a result of three main sources of friction. Coulomb friction, which results from the friction of the moving parts in the WEC assembly. In this case this is the friction between the linear translator and its supporting structure. The second source is viscous friction which is a result of the friction due to the air gap between the stator windings and the translator. Finally, the Stribeck effect is considered which results from the force needed to move a resting body. The equation representing this force is [22]:

$$f_f(t) = \alpha_c sign\big(v(t)\big) + \alpha_v(t) + (\alpha_s - \alpha_c)e^{-(v(t)/v_s)} sign\big(v(t)\big) \tag{2.16}$$

2.1.7 Radiation Force

Whenever the buoy moves linearly vertical to the water surface, waves are induced and generated away from it. Forces are applied to the submerged part of the buoy as a result and this force is referred to as radiation force $f_r(t)$ [36]. The approach to modeling

the radiation force is similar to the modeling of the excitation force. The time domain equation for the radiation force is [37]:

$$f_r(t) = -m_\infty a(t) - \int_0^t k_r(t-\tau)v(\tau)\,d\tau \tag{2.17}$$

where m_∞ is the body added mass at infinite frequency [22], and $a(t)$ is the heave acceleration. The integration part of the equation represents the energy dissipated by the radiated waves and the inertial energy of the water around the submerged surface of the buoy. It is clear that this term would only exist while the buoy is moving, therefore convolution of the radiation impulse response function and the buoy velocity is present in the equation.

The radiation frequency impulse response function $K_r(t)$ can be related to the radiation resistance or damping in the frequency domain, as well as to the radiation added mass. The radiation resistance or damping $R_r(\omega)$, from its name, is the energy dissipation term. While the radiation added mass is associated with the body physical mass of the buoy as an added inertia term [22][27]:

$$R_r(w) = \int_0^\infty K_r(t)cos(\omega t)dt, \tag{2.18}$$

$$M_r(\omega) = m_\infty - \frac{1}{\omega}\int_0^\infty K_r(t)sin(\omega t)dt \tag{2.19}$$

The inverse Fourier transform and $R_r(\omega)$ are used to end up with the expression shown below:

$$K_r(t) = \frac{2}{\pi}\int_0^\infty R_r(w)cos(\omega t)d\omega \tag{2.20}$$

where by using Euler's formula and equations 2.18 and 2.19 we end up with:

$$K_r(i\omega) = R_r(\omega) + i\omega[M_r(\omega) - m_\infty] \tag{2.21}$$

By performing Fourier transform on equation 2.17 and using 2.21 in that expression we get the expression for the radiation force:

$$F_r(i\omega) = -[R_r(\omega) + i\omega M(\omega)]V(i\omega) \tag{2.22}$$

$V(i\omega)$ is the Fourier transform of velocity. Similar to the excitation force, WAMIT is used to generate radiation resistance and added mass data shown in Figure 7.

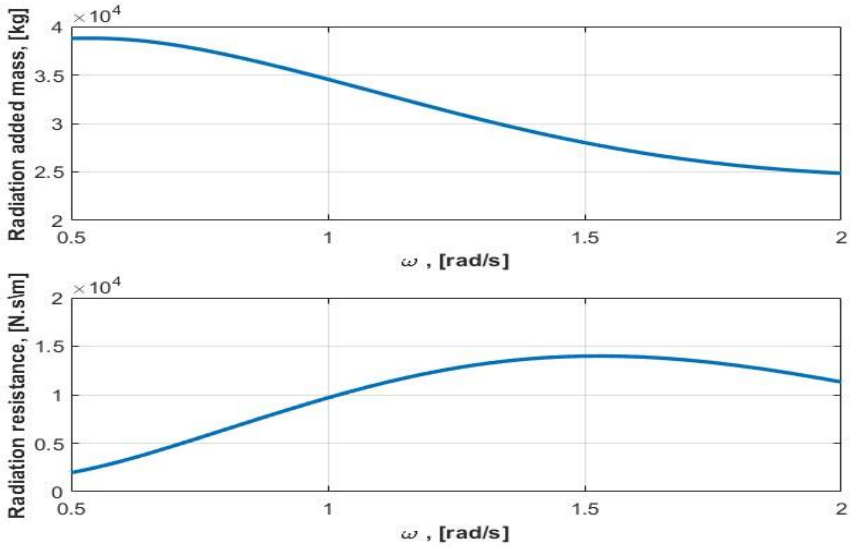

Figure 7: WAMIT generated data for the radiation resistance and radiation added mass in frequency domain

"invfreqs" is used to find a Laplace transfer function. The unstable poles are also mirrored to ensure stability and the order of n is found by experiment (iterative methods). The approximated $K_r(s)$ is:

$$K_r(s) = 1 \times 10^4 \frac{1.475s^3 + 5.292s^2 + 4.115s}{s^4 + 3.291s^3 + 7.946s^2 + 7.707s + 4.227} \tag{2.23}$$

It can be observed from Figure 8 that the poles are stable, Figure 9 shows how close the approximation fits the data:

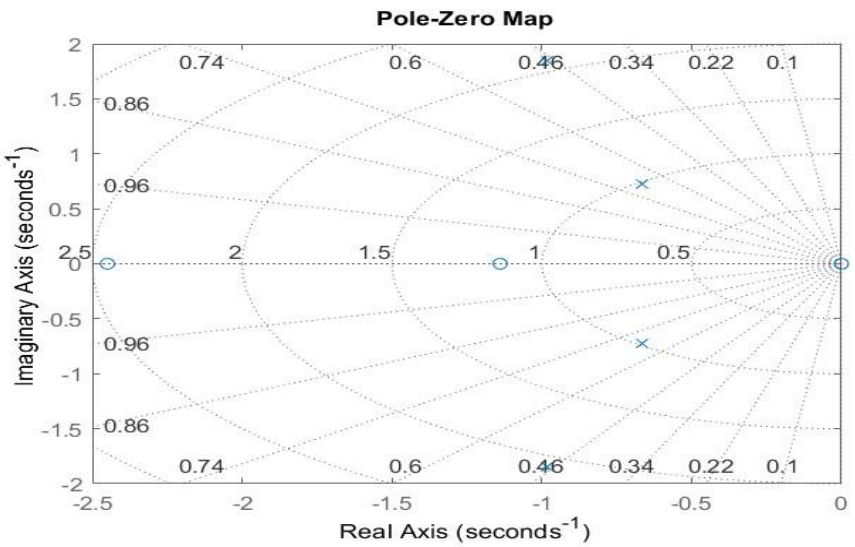

Figure 8: Pole-zero map for the cylindrical buoy

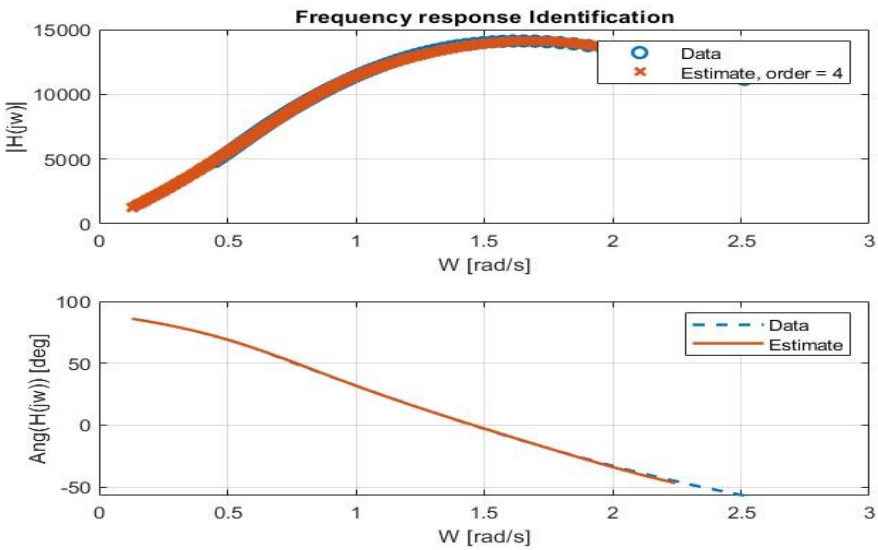

Figure 9: The magnitude and phase angle of the radiation frequency response function for the cylindrical buoy

Finally, and similar to the excitation force, "tf2ss" was used to find the state space representation of the radiation force to be used in Simulink.

2.1.8 Electromagnetic force

The part of the machine responsible for converting the mechanical force into another form of energy, in this case electrical, is called the Power Take-off (PTO) mechanism. In this context, the PMLG is the electrical direct drive PTO mechanism direct

drive means that the linear translator is driven directly by the motion of the buoy with the waves. Maximum power absorption is achieved if the device is moving in resonance with the sea waves.

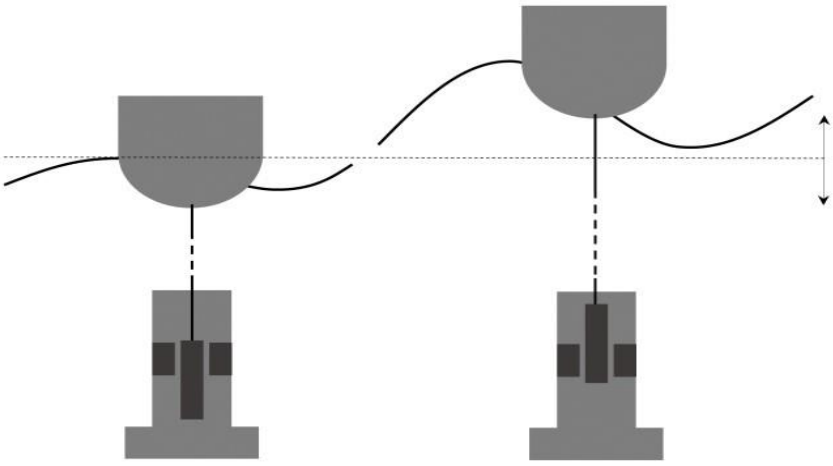

Figure 10: Direct drive principle [22]

Proper control of this mechanism can lead to increase in the efficiency of the PTO mechanism, increasing power absorption [38].

The PTO mechanism consists of all the forces that affect the motion of the floating buoy. Therefore, that consists of the electromagnetic/control force, restoring force, friction force and end-stop force:

$$f_{pto} = f_u + f_{rs} + f_f + f_{es} \tag{2.24}$$

where f_{pto} is the power take-off force. forces other than the control force are discussed later.

Similar to synchronous rotary machines, the linear translator of the PMLG induces electromotive force in the stator windings based on Faraday's Law [22][39]. Current flowing in the stator windings results in an opposite magnetic flux to that generated by the permanent magnet which is referred to as the armature reaction. Therefore, varying the voltage at the stators means that the armature reaction can be controlled, hence, calling the

electromagnetic force the control force. Varying the voltage at the stators can be done using power converters [22][40].

The control force, which is proportional to the stator current can be expressed as:

$$f_u = \frac{3\pi}{2p_\omega}\lambda_{pm} i_{sq} \tag{2.25}$$

where p_ω is the machine pole pitch, λ_{pm} is the permanent magnet flux, and i_{sq} is the quadrature component of the machine stator current.

It is also important to note that slower speeds lead to maintaining higher forces which works well for heaving WECs [41][22].

The simple and passive control technique that was initially used to simulate the model is called Resistive Loading (RL). in RL, the aim is to produce a linearly proportional control force compared to the heave velocity [22][23]. The reference control force in this method is simply, yet sub-optimally, represented as [22]:

$$\tilde{f_u} = -R_c(\omega)v(t) \tag{2.26}$$

where R_c is a frequency dependent resistance that can be determine using the magnitude of the system intrinsic impedance:

$$R_c(\omega) = |Z_{int}(\omega)| = \sqrt{\left(R_{int}(\omega)\right)^2 + \left(X_{int}(\omega)\right)^2} \tag{2.27}$$

$R_{int}(\omega)$ and $X_{int}(\omega)$ are the resistive and reactive components of the system intrinsic impedance. The resistive component is equal to the radiation resistance:

$$R_{int}(\omega) = R_r(\omega) \tag{2.28}$$

where the reactive component is:

$$X_{int}(\omega) = \omega(m + m_\infty + M_r(\omega)) - \frac{(C_b + S_r)}{\omega} \tag{2.29}$$

This representation of $R_c(t)$ causes it to be large, which means the buoy motion is conservative. In addition to that, Resistive loading assumes uni-directional power flow, as in both the excitation force and heave velocity are in phase due to the absence of a reactive component [22]. However, this leads to better utilization of the PTO resource due to low (better) peak-to-average ratios [42][36]. As mentioned earlier, requirement of a real-time knowledge of the wave frequency makes this solution sub-optimal since it will be tuned to a single frequency (dominant wave frequency).

Reactive Control (RC) or Approximate Complex Conjugate control is an active control strategy that enables bidirectional power flow by considering the damping and stiffness coefficients of the springs. In [23] the reference control force is represented as:

$$\hat{f}_u = -R_{pto}v(t) - K_{pto}z(t) \tag{2.30}$$

where R_{pto} is the spring damping coefficient, K_{pto} is the spring stiffness coefficient and $v(t), z(t)$ are the velocity and displacement of the buoy respectively. By including copper losses in the control strategy, the spring damping coefficient can be expressed as:

$$R_{pto} = \frac{R_r(\omega) + 2\delta[R_r^2(\omega) + X_{int}^2(\omega)]}{\gamma(\omega)} \tag{2.31}$$

δ and γ(ω) are auxiliary variables that include the effect of copper losses and can be expressed as:

$$\delta = \frac{2p_\omega^2}{3\pi^2\psi_{pm}^2}R_s \tag{2.32}$$

where R_s is the stator resistance and ψ_{pm} is the flux linkage amplitude of the translator's permanent magnets. γ(ω) is expressed as:

$$\gamma(\omega) = 4\delta^2[R_r^2(\omega) + X_{int}^2(\omega)] + 4\delta M_r(\omega) + 1 \tag{2.33}$$

The intrinsic reactance is expressed as:

$$X_{int}(\omega) = \omega(m + M_r(\omega)) - \frac{C_b + S_r}{\omega} \tag{2.34}$$

whereas the stiffness spring coefficient is expressed as:

$$K_{pto} = \frac{\omega X_{int}}{\gamma(\omega)} \tag{2.35}$$

The presence of the reactive component of the intrinsic impedance implies the bi-directional power flow. The polynomial coefficients of the radiation resistance and radiation added mass were found as mentioned in section 2.1.6.

Finally, [23] assumes the use of peak frequencies in all the equations above.

2.1.9 Section Summary

To summarize, the methodology discussed in this section was used to model each one of the forces into Simulink, excluding friction force and end-stop force. Resistive loading was used as an initial method of simulating the operation of the wave energy converters, but Reactive control (Approximate Conjugate Control) is used as a basis for the upcoming improvements. The workflow can be summarized in the following points:

- Buoy parameters, state-space models and function estimations are done in MATLAB.
- Relevant parameters are saved in the MATLAB workspace.
- Simulink uses the relevant parameters in the workspace to perform the simulation.

The Simulink implementations of the WEC model, resistive loading & reactive control can be seen in Figure 23, Figure 24 & Figure 25.

2.2 Machine Side Converter Controller & PMLG System

The Machine Side Converter Controller (MSCC) block described in this section is simulated in MATLAB & Simulink with the purpose of:

- Ensure that the control force is tracking the reference control force.
- Calculate the d-q reference frame voltages of the stator windings.

2.2.1 Machine Side Converter Controller

Based on Equation 2.25, the reference stator quadrature current can be calculated. To ensure proper tracking, a PI controller is implemented.

Implementation of a PI controller is based on the following equation for the direct current of the stator [43][39]:

$$v_{sd}(t) = R_s i_{sd}(t) + L_s \frac{di_{sd}}{dt} - \omega_e L_s i_{sq}(t) \tag{2.36}$$

with ω_e equal to [22]:

$$\omega_e = \frac{\pi v(t)}{p_w} \tag{2.37}$$

According to [43], an auxiliary control variable was introduced and can be represented as:

$$\frac{di_{sd}}{dt} = -\frac{1}{\tau_\sigma} i_{sd}(t) + \frac{1}{\tau_\sigma r_\sigma} \tilde{u}_{sd}(t) \tag{2.38}$$

where tilde means the reference auxiliary variable. By rearranging the equation, we end up with:

$$\tilde{u}_{sd}(t) = \tau_\sigma r_\sigma \frac{di_{sd}}{dt} + \frac{1}{\tau_\sigma} i_{sd}(t) \tag{2.39}$$

The transfer function between the reference voltage and the current is:

$$\frac{I_{sd}(s)}{\tilde{U}_{sd}(s)} = \frac{\frac{1}{\tau_\sigma r_\sigma}}{s + \frac{1}{\tau_\sigma}} = \frac{b}{s+a} \tag{2.40}$$

where the PI controller parameters:

$$K_p^d = \frac{2\zeta\omega_n - a}{b}, \tau^d = \frac{2\zeta\omega_n - a}{\omega_n^2} \tag{2.41}$$

These can be found based on parameters proposed by the book:

$$a = \frac{R_s}{L_s}, b = \frac{1}{L_s}, \zeta = 0.707, \omega_n = \frac{1}{1-0.95} a \tag{2.42}$$

Where the real value of the variable is found using the PI controller as:

$$u_{sd} = K_p^d(i_{sd}^*(t) - i_{sd}(t)) + \frac{K_p^d}{\tau^d}\int_0^t (i_{sd}^*(t) - i_{sd}(t))d\tau \tag{2.43}$$

By looking at equations 2.36 & 2.39, we can notice the relationship between the direct voltage of the stator and the auxiliary variable where:

$$v_{sd}(t) = \frac{\pi}{p_w} L_s i_{sq} - u_{sd}(t) \tag{2.44}$$

This fulfills part of the second goal of the MSCC. To fulfill the goal entirely the same procedure is repeated to find the quadrature stator current where:

$$v_{sq}(t) = R_s i_{sq}(t) + L_s \frac{di_{sq}}{dt} - \omega_e L_s i_{sd}(t) + \omega_e \psi_{pm} \tag{2.45}$$

and repeating the previous steps. The Simulink block representing the controller is shown in Figure 11:

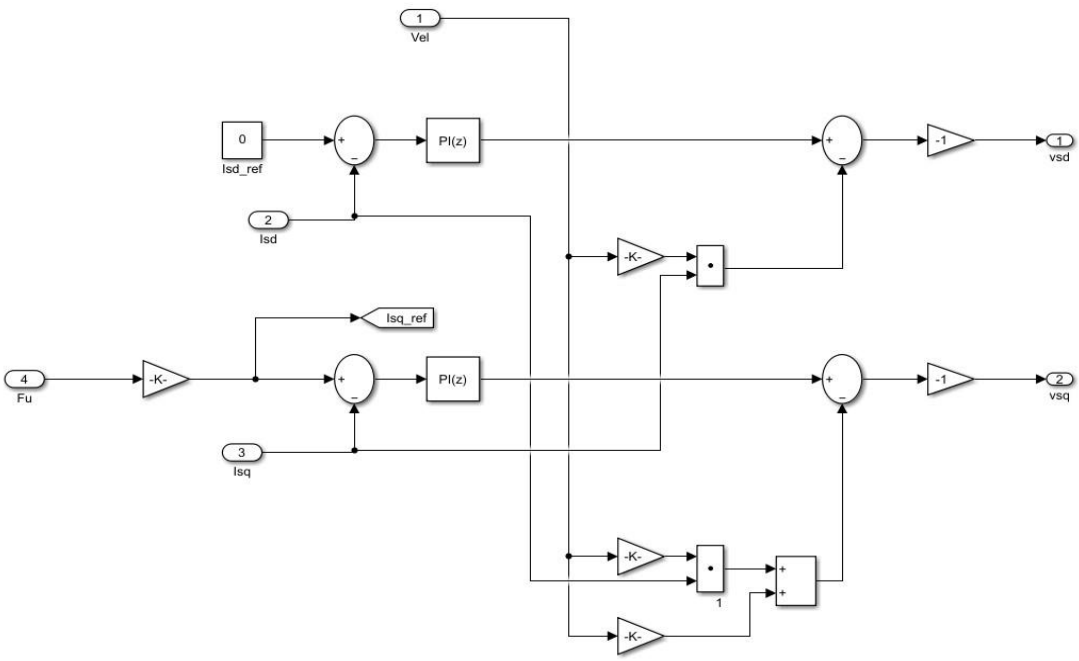

Figure 11: Simulink block for the MSCC

The direct current value is set to zero to minimize copper losses [44]. The values of direct and quadrature components of the stator current will be acquired from the PMLG System Block.

2.2.2 PMLG System

By rearranging equation 2.36 [39]:

$$\frac{di_{sd}}{dt} = -\frac{v_{sd}(t)}{L_s} - \frac{R_s}{L_s} i_{sd}(t) + \omega_e i_{sq}(t) v(t) \tag{2.46}$$

where the definition of the differentiation term can be expressed as follows:

$$\frac{di_{sd}}{dt} = \frac{i_{sd}(t) - i_{sd}(t-1)}{T_s} \tag{2.47}$$

T_s is the sampling time which can also be referred to as Δt. Rearranging once again will result in the following expression:

$$i_{sd}(t) = i_{sd}(t-1) T_s \left(-\frac{v_{sd}(t)}{L_s} - \frac{R_s}{L_s} i_{sd}(t) + \omega_e i_{sq}(t) v(t)\right) \tag{2.48}$$

Therefore, acquiring the real values of the direct stator current that is used in the MSCC Block. This procedure is repeated for the quadrature current using equation 2.45. Finally, white gaussian noise is added to the signal. The Simulink block representing the controller is shown in Figure 12:

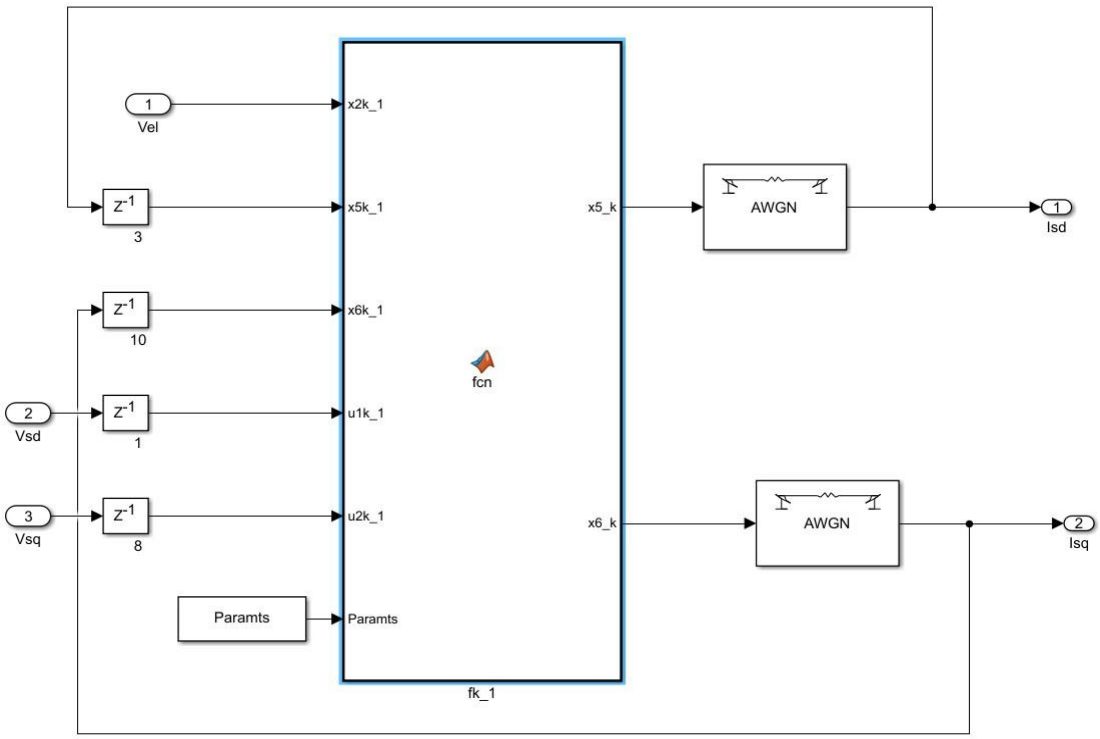

Figure 12: Simulink block for the PMLG System

where the values of the direct and quadrature components of the stator voltage are acquired from the MSCC Block. The function block handles the mathematical operations needed in this part and Paramts block provides the constants needed.

2.3 Analysis Block

The Analysis block model described in this section is simulated in MATLAB & Simulink with the purpose of:

- Calculate the real value of the control force.
- Calculate the average electrical & electromagnetic power generated of the system.
- Calculate the electrical and & electromagnetic energy generated by the system.
- Find the efficiency of the PMLG.

The real value of the control force can be found through equation 2.25 by using the real value of the stator quadrature current found in the previous section. However, this power is to be saturated due to the limitations of the machine. The maximum value of the control force is set to 1.5MN. Similarly, the reference control force has to be saturated as well.

The instantaneous mechanical power generated by the system is obtained by:

$$P_m = f_u(t)v(t) \tag{2.49}$$

The running mean is calculated to find the average power during the simulation. The electromagnetic energy by definition is the integration of the instantaneous power:

$$E_m = \int_0^t f_u(\tau)v(\tau)d\tau \tag{2.50}$$

The instantaneous electrical power can be obtained by:

$$P_e = \frac{3}{2}[v_{sd}(t)i_{sd}(t) + v_{sq}(t)i_{sq}(t)] \tag{2.51}$$

Similarly, the running mean of the electrical instantaneous power is calculated as well as the electrical energy:

$$E_e = \int_0^t \frac{3}{2}[v_{sd}(\tau)i_{sd}(\tau) + v_{sq}(\tau)i_{sq}(\tau)]d\tau \tag{2.52}$$

Finally, the efficiency of the PMLG is calculated as the ratio between the electrical energy and the electromagnetic energy.

$$\eta_{pmlg} = \frac{E_e}{E_m} \tag{2.53}$$

2.4 Sea state estimation using Recurrent Neural Networks

This section discusses a novel method of predicting sea states in real time. Most of the equations and/or control techniques require a real time measurement of wave frequency. In addition, wave significant height can be useful in reactive control techniques that use look up tables with H_{hw} & T_{hw} as entries.

Current techniques of predicting the sea state require collecting measurements for a period of time from a separate buoy, then applying the statistical definition of wave height and wave period to find the dominant sea state. That might not be ideal since it does not deal with wave components on a crest to trough basis for irregular waves. The proposed method theorizes that if each crest or trough can be dealt with separately and controlled in real time, then optimal control can be applied on individual crest/trough basis rather than a statistical average. Therefore, for irregular waves, peaks that do not occur as usual compared to the dominant wave height can be controlled for optimal power absorption individually. The statistical definition is mentioned in Section 1.2. However, the proposed definition can be seen in Figure 13.

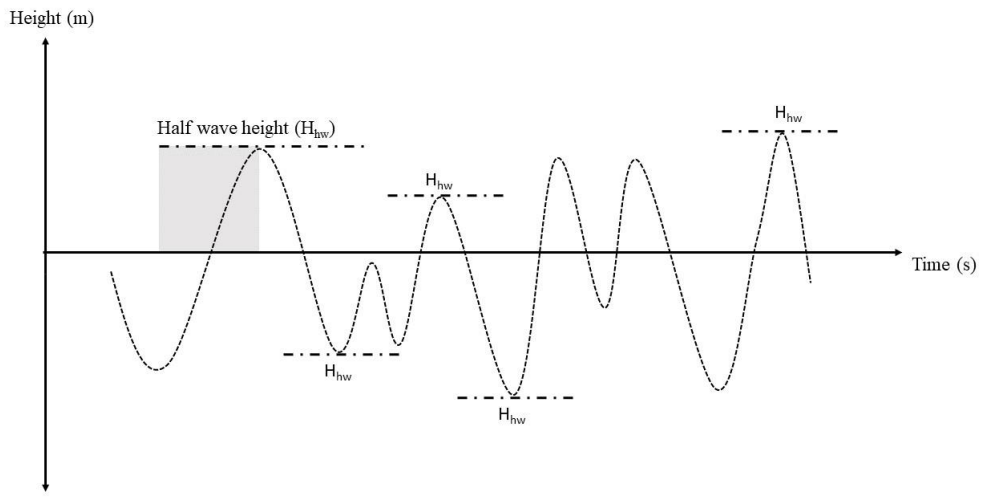

Figure 13: Half-Wave Height described in irregular waves

As seen in Figure 13, half-wave is defined as the positive or negative slope leading to a peak or a trough after crossing calm sea level. In the case of wave period, for a half-wave the period is defined as the period of the regular wave representation of this half-wave. Meaning that if this wave form was regular, then the wave period would be between two crests or two troughs.

This leads to the need of estimation or prediction techniques to make use of the half-wave data leading to H_{hw} or T_{hw}. Using a Kalman filter can predict one time step ahead using previous data, meaning it might be able to predict the next point on the slope rather than the end peak[45]. However, Recurrent Neural Networks (RNN) are a class of neural networks capable of predicting an output based on time series data where that can or can not be the next time step. The capabilities of RNNs in time series forecasting and performance comparisons between RNNs and Kalman filters have been highlighted in research [46][47]. Therefore, this technique was chosen to handle the task at hand.

2.4.1 Data Collection

Data is one of the main determinants of neural network performance. In order to make sure a neural network is able to output correct predictions, the data set needs to include enough features and variance for the neural network to be able to generalize the solution. Hence, understanding the non-linear relationship between inputs and outputs. Iterative trial and error were used to reach the optimal data set in this work. Different inputs define different datasets and based on that they can be split as described below:

- The sea state is varied by 1 m in half wave height and 1 s in half wave period. Data is collected from regular waves.
- The number of sea states is either 9 or 25.
- Sampling time varied between 0.2 s or 1 s. In either case, 4 samples are collected as time-series input to the recurrent neural network.
- The output is half wave height, half wave period, and both. The final choice is discussed in the architecture section.
- Inputs are:

- Buoy displacement.
- Buoy velocity.
- Buoy acceleration.
- Damping coefficient R_{pto}.
- Stiffness coefficient K_{pto}, combinations are applied similar to the damping coefficient.
- Control force.

Combinations of these parameters have been experimented with as inputs.A sample of the Data Collection Simulink block is shown in Figure 14.

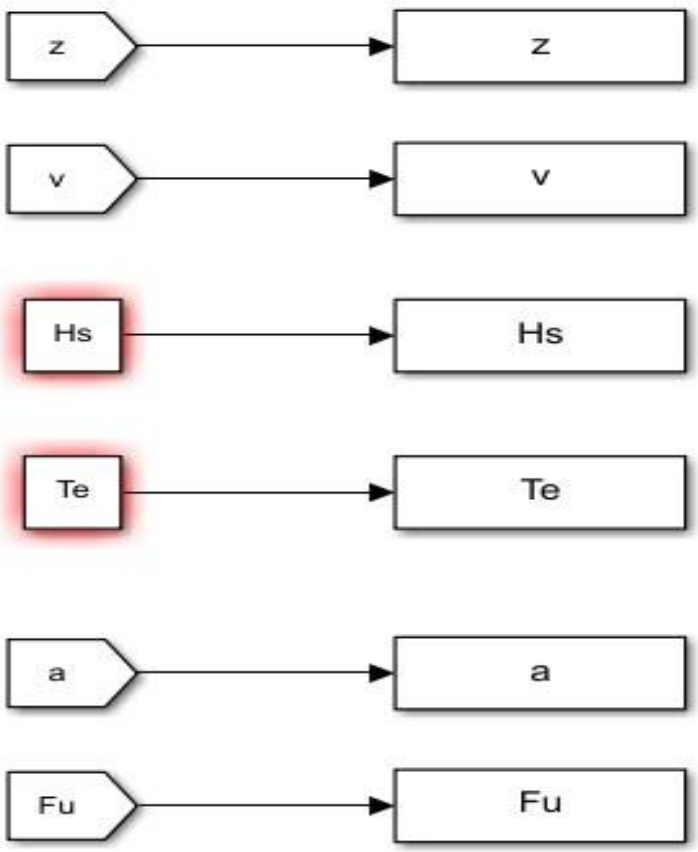

Figure 14: Data Collection Block for datasets including maximum buoy displacement as output

After trials, sampling time was chosen to be 0.2 s. This means that collecting 4 data samples would take 0.8 s to output a prediction. Simulation time is 200 s, meaning that data for H_{hw} and T_{hw} was collected from a simulation of regular sea states for 200 s. The data is only collected after 100 seconds of simulation due to initial transients. The main data set chosen for comparison consists of the absolute value of buoy displacement and absolute value of buoy velocity. The output of this stage is the H_{hw} and T_{hw}. 80% of the data is used for training, the rest is used for validation. These datasets are collected in 9 sea states.

- H_{hw} varying between 1-3 m.
- T_{hw} varying between 8-10 s.

Time series data is collected from regular waves (training data) using the optimized look up table approach described in the next section, and 5% of the data is used a testing set. Batch size is set to 128 due to the size of the data set while the network is trained for 10000 epochs. The trained model will be deployed in both regular and irregular sea states for evaluation. The main idea is that learning the sea state of regular waves can lead to learning half-wave states in irregular waves.

2.4.2 Recurrent Neural Network Architecture

The input layer of the RNN is chosen based on input size, additionally the inputs are normalized by their mean and standard deviation (zscore). Similarly, the output layer is chosen based on the outputs. It consists of a regression layer preceded by a fully connected layer. In the case of one output, the fully connected layer would have one output, and in the case of two outputs it would have two. However, careful choice of the hidden layers is necessary to ensure learning. The more features or unique inputs are expected, the more the number of hidden neurons [48]. This does not correspond to increasing the number of hidden neurons infinitely, since that will also lead to higher computational times and cause over-fitting [49]. Therefore, a Long Short Term Memory (LSTM) layer based neural network was chose. The proposed architecture can be seen in Figure 26. The output of this neural network is then rounded to the nearest integer to use as an input for the look up tables mentioned in the next section. Additionally, GRU layers

were also experimented with using the same number of hidden neurons. In all cases, Adam optimizer was chosen by default for all cases [50].

LSTM was proposed in 1997 to solve the issue of storing information over periods of time. Specifically, the long computation times due to insufficient error backflow [51]. Therefore, LSTM was proposed to have a short term memory that can work for longer periods of time. Hence, calling it LSTM. The advantages that LSTM carries are the insensitivity to the gap between steps and dealing with the issue of vanishing gradient [51]. This makes it ideal for the current application since the time step is 0.2 s.

The main difference between GRU & LSTM is the forward step calculation. That is dependent on the operation of neurons. The neuron is described in Figure 15.

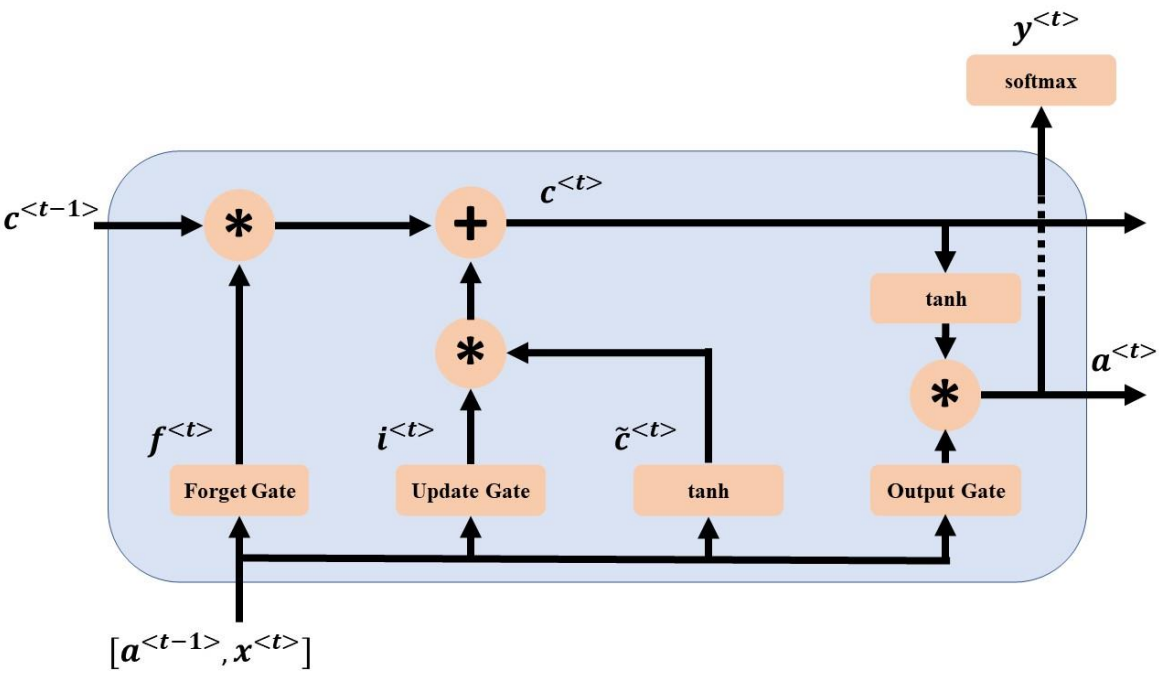

Figure 15: I/O diagram of LSTM Neuron [52]

$x^{<t>}$ is the current time step of the input, which makes $x^{<t-1>}$ the previous time step of the input. The memory cell output is $c^{<t>}$. $a^{<t>}$ is the activation output of the current cell, and $c^{\sim<t>}$ is the candidate memory cell output. Finally $y^{<t>}$ is the prediction at this time step. However, the output mode of the LSTM layer is set to "last" to only get the prediction of the final cell. The equations governing the operation of the cell are:

$$
\begin{aligned}
\tilde{c}^{<t>} &= tanh(W_c[a^{<t-1>}, x^{<t>}] + b_c) \\
\Gamma_u &= \sigma(W_u[a^{<t-1>}, x^{<t>}] + b_u) \\
\Gamma_f &= \sigma\big(W_f[a^{<t-1>}, x^{<t>}] + b_f\big) \\
\Gamma_o &= \sigma(W_o[a^{<t-1>}, x^{<t>}] + b_o) \\
c^{<t>} &= \Gamma_u * \tilde{c}^{<t>} + \Gamma_f * c^{<t-1>} \\
a^{<t>} &= \Gamma_o * tanh(c^{<t>})
\end{aligned}
\tag{2.54}
$$

where W_c is the hyperparameter matrix. This longer version of the simplified notation is:

$$
\begin{aligned}
W_c &= [W_{ca} \quad W_{cx}] \\
W_c[a^{<t-1>}, x^{<t>}] &= [W_{ca} \quad W_{cx}] \begin{bmatrix} a^{<t-1>} \\ x^{<t>} \end{bmatrix}
\end{aligned}
\tag{2.55}
$$

Finally, b is the bias parameter that is usually set to 0 or 1. This notation is used similarly for all of the hyperparameter matrices.

The intuition here is that by having both an update and a forget gate in the cell output, there is the option of keeping the old value and adding to it or forgetting it. This is due to the forget gate and update gate outputs being 1 or 0 most of the time [53][52][51].

Gated Recurrent Units (GRU) were first proposed in 2014 in comparison with RNN Encoder-Decoder methods [54]. Similar to LSTM, the GRU is capable of handling the vanishing gradient issue. An application of GRU is being able to provide context in a sentence. In longer sentences where the subject (singular or plural) is early, GRU can determine whether to use a singular or plural verb [55]. By intuition, this type of neural network should be able to assist in predicting Half-wave height while keeping the earlier time steps in consideration. The GRU neuron is described in Figure 16.

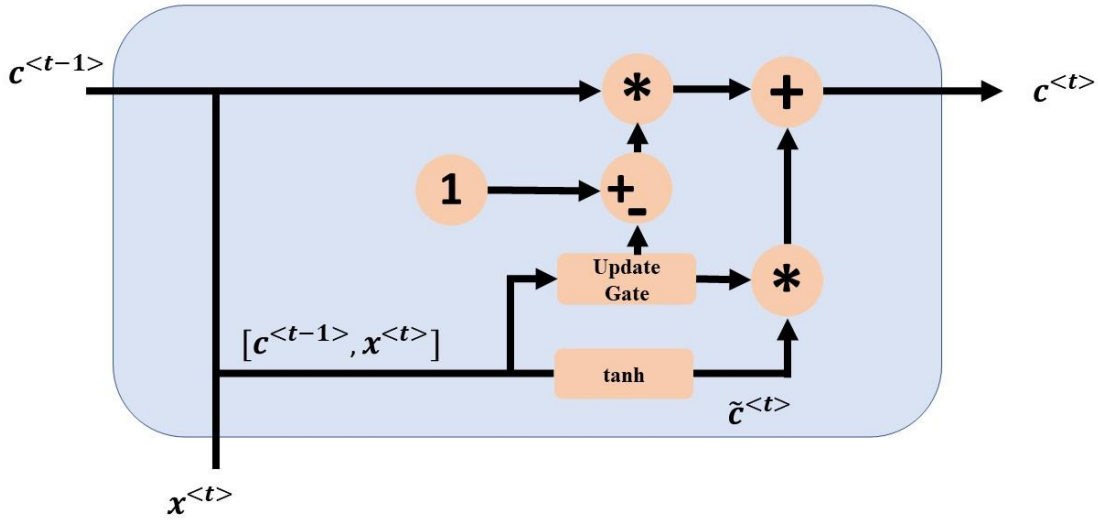

Figure 16: I/O diagram of GRU Neuron [55]

The same notation used in LSTM is used here. The main difference is the presence of one gate (update gate) to determine presence (or lack of) context from previous memory cells. The equations governing the operation of a GRU neuron are:

$$\begin{aligned} \tilde{c}^{<t>} &= tanh(W_c[c^{<t-1>}, x^{<t>}] + b_c) \\ \Gamma_u &= \sigma(W_u[c^{<t-1>}, x^{<t>}] + b_u) \\ c^{<t>} &= \Gamma_u * \tilde{c}^{<t>} + (1 - \Gamma_u) * c^{<t-1>} \end{aligned} \tag{2.56}$$

After training is complete, the model is imported into Simulink using the predict block which outputs a prediction at every time steps. Therefore, data was arranged similar to the training set before feeding into the network. This is done using Function and Delay blocks. The block is shown in Figure 17. Remark that this architecture only requires the displacement and velocity as input, which solves any issues with algebraic loops caused by other inputs.

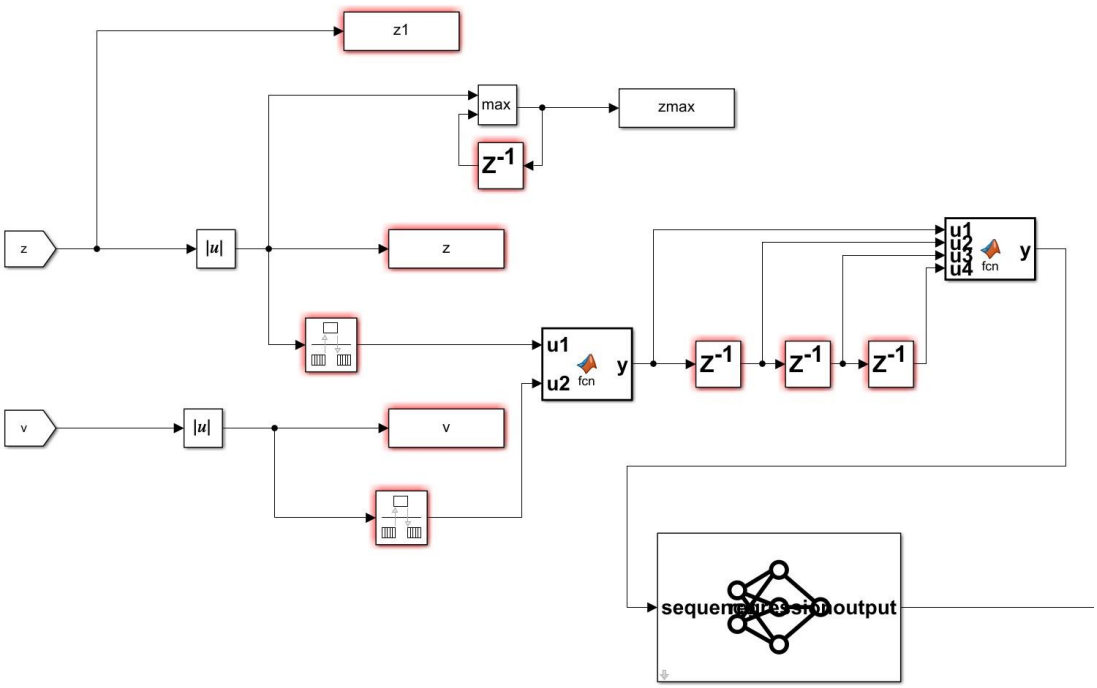

Figure 17: Simulink block of RNN deployment

2.5 Reactive Control using Neural Networks

The work in this section aims to improve the power absorption using reactive control adopted from the International Journal of Marine Energy [16]. This method uses feed forward neural networks (a.k.a artificial neural networks (ANN)) as a cost function in conjunction with a global optimization algorithm. A The proposed neural network architecture consists of the inputs.

- Half Wave Height H_{hw}.
- Half Wave Period T_{hw}.
- Damping Coefficient R_{pto}
- Stiffness Coefficient K_{pto}

The inputs are chosen based on the dataset collected for the RNNs in the previous section. These inputs are fed to two hidden layers of 10 neurons each to construct two identical single output feed forward NNs. The hidden layers use a tanh activation function while the output uses a regression layer. The outputs are the average electrical power

generated by the device and maximum displacement experienced by the buoy. This architecture is shown in Figure 18.

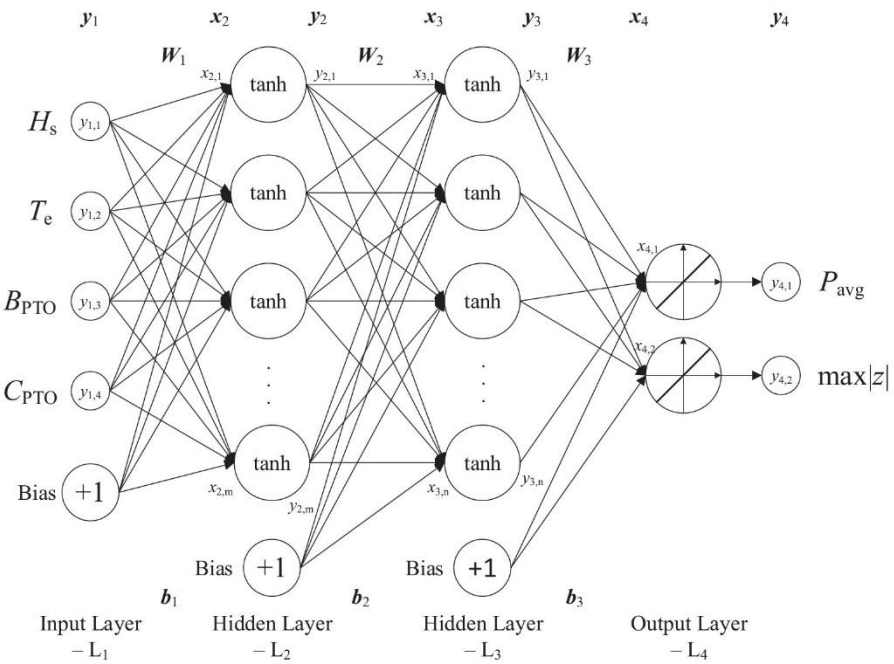

Figure 18: Feed forward NN architecture for the optimization algorithm as described by the original paper [16]

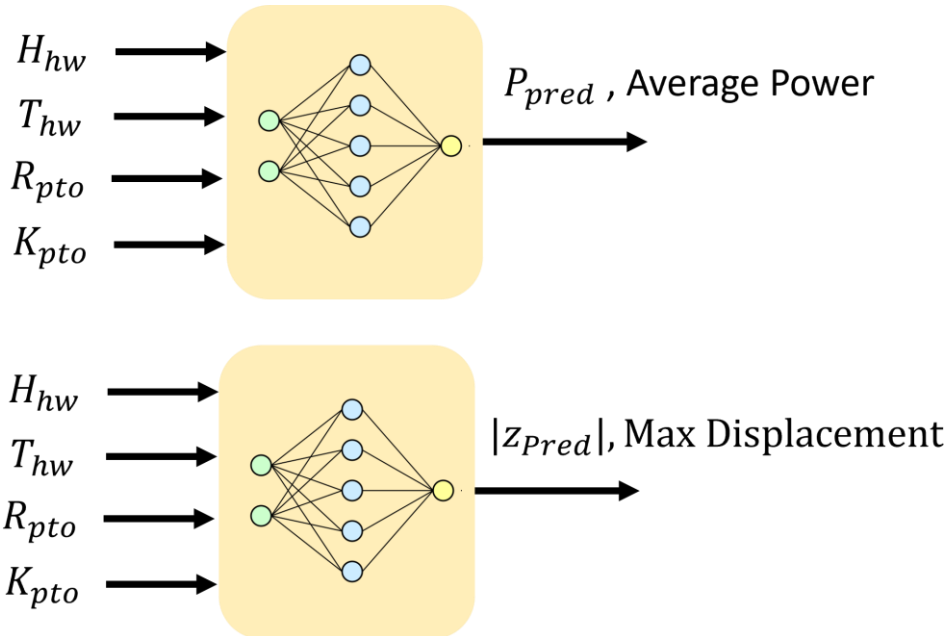

Figure 19: Implementation used in this work of the network in Figure 18 [16]

The original paper used one neural network for both outputs. However, for ease of implementation in the cost function, these networks were split into two. Inputs are

normalized by mean and standard deviation and training is done using batch mode rather than a single example at a time. Since the network will be later on used to generate look up tables to be used by the estimation networks. Finally, the neural networks use typical forward and backward propagation as described in [49]. The authors of this method proposed using a MultiStart optimization algorithm [56] for a minimization problem. This is done using "fmincon" (minimization) in MATLAB with a 100 random starting points. The cost function is.

$$cost = \left\{ \begin{array}{ll} -P_{pred}, & |z_{pred}| \leq z_{Max} \\ +1, & |z_{pred}| > z_{Max} \end{array} \right\} \tag{2.57}$$

Where P_{pred} and z_{pred} are the predicted average power and predicted displacement by the ANN. The main idea is to explore different choices of coefficients that might possibly increase power absorption as long as they maintain the physical constraints. The constraints are also enforced by having the damping and stiffness coefficients limited in a range. The data collection and training loop can be seen in Figure 20.

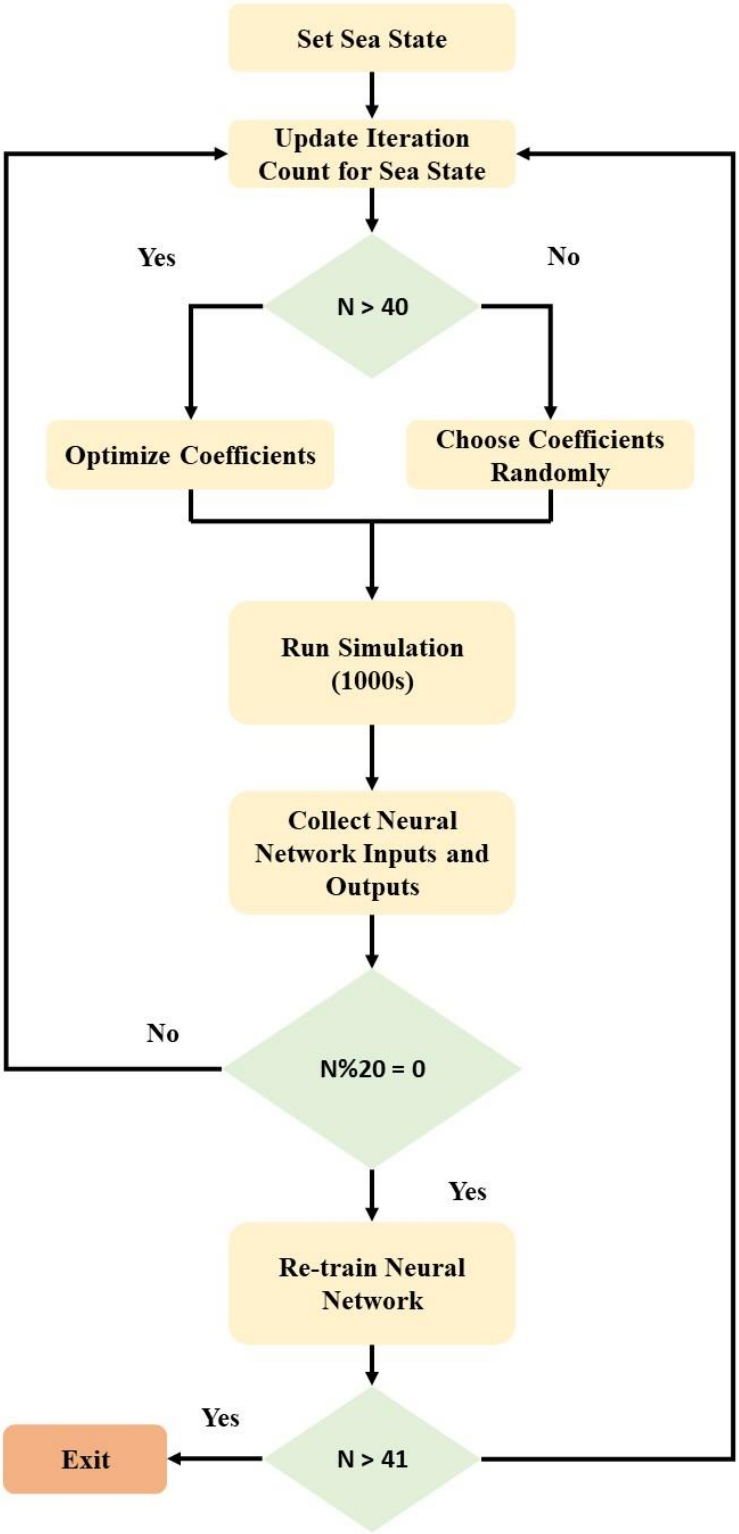

Figure 20: Flow chart of the ANN training and data collection

The flow is as follows:

1. Sea state is chosen.
2. Update the iteration count N for the sea state.
3. If the sea state has been visited less than 40 times, the damping and stiffness coefficients are chosen randomly within a search space.

$$R_{pto} = R_{pto,opt} + \Delta R_{pto}$$
$$\Delta R_{pto} = (r - 0.5) * range(R_{pto}) * 0.9^{N-40} \qquad (2.58)$$

Where ΔR_{pto} is a randomization window that minimally changes the output of the optimization to allow for exploration around the optimal value. The last term causes the exploration window to decrease as more iterations go by. The same is applied to K_{pto}.

4. The simulation is run for 1000 seconds, since this is the time required to ensure the average power reading is almost constant.
5. Input and output vectors are collected. The network is trained every 20 iterations on the accumulated collected data.
6. Once the number of iterations passes 41, the optimal coefficients are found and the loop exits. The reason only 41 iterations are considered is to save on computational time. In the original paper, any iterations after that are for exploration around the optimal coefficients for online continuous learning.

Finally, the optimal values of the coefficients are used to create a look up table, which is used for training the RNNs, in Simulink as shown in Figure 21.

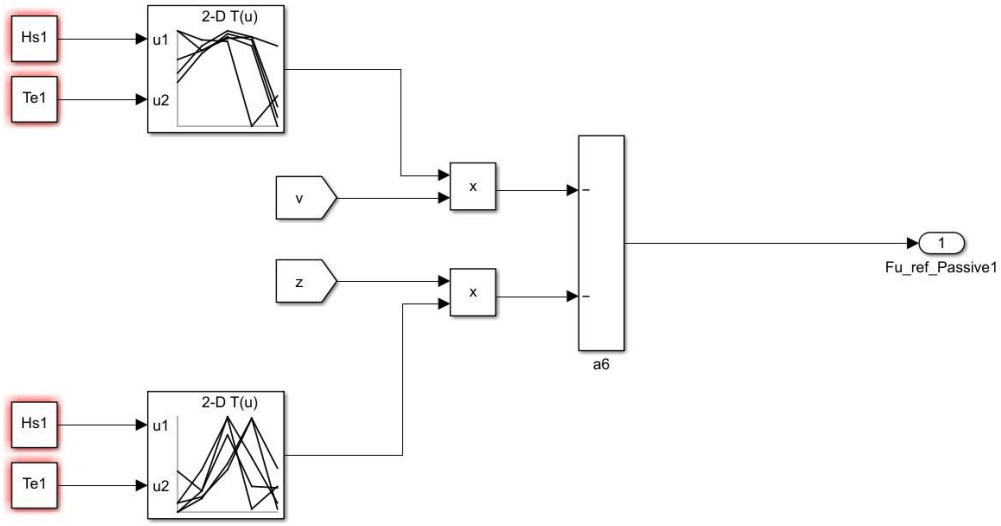

Figure 21: Simulink Block of reactive control using look up tables

Additionally, the final control method consists of a combination of the prediction network and the look up tables, which can be seen in Figure 22.

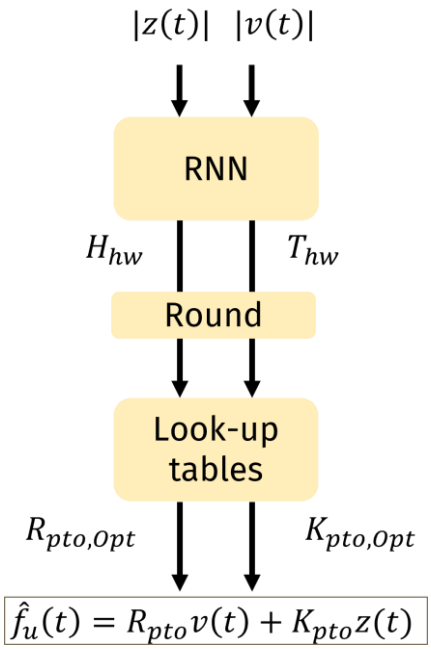

Figure 22: Fully neural network based controller

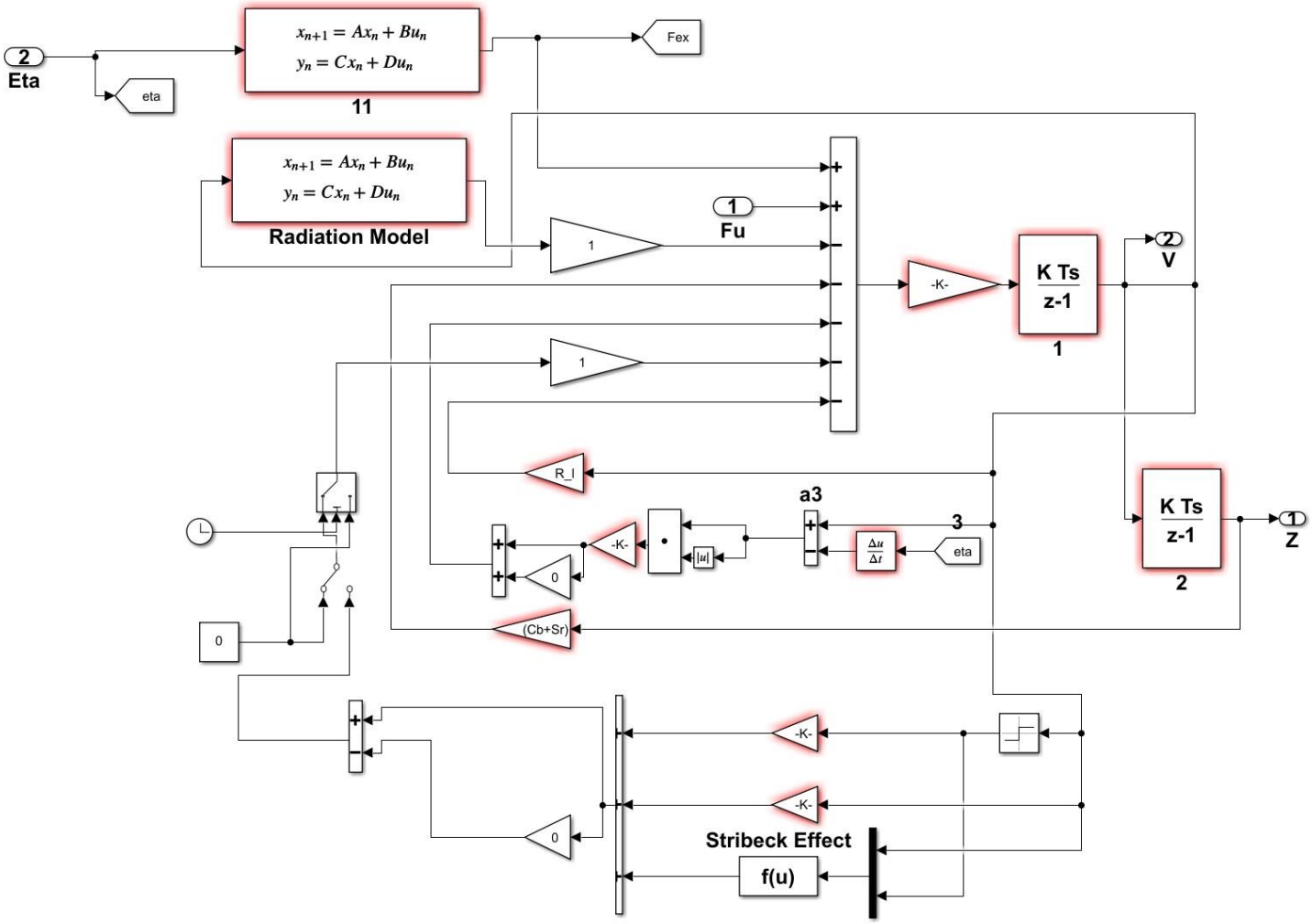

Figure 23: Simulink block for the WEC model

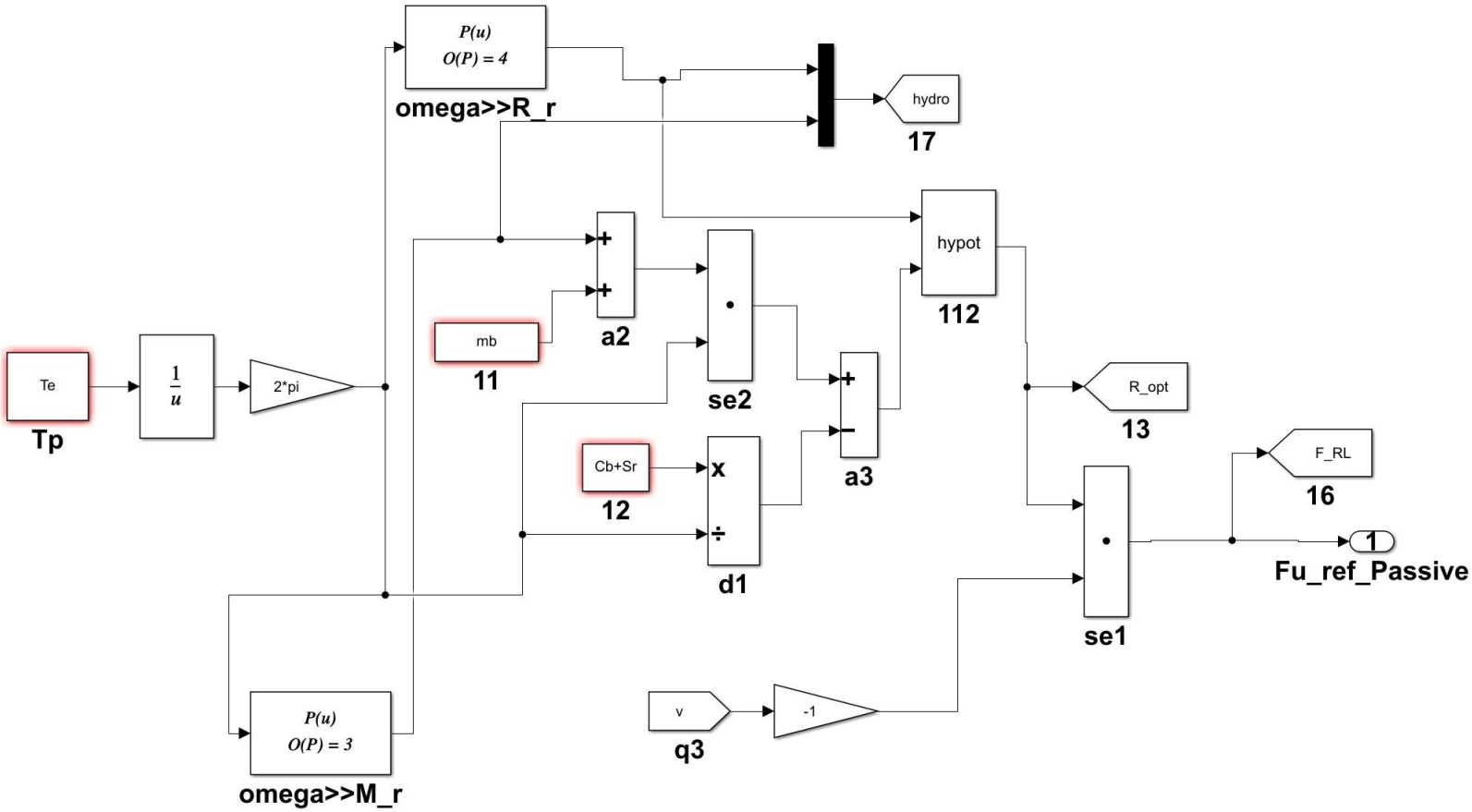

Figure 24: Simulink block for Resistive Loading

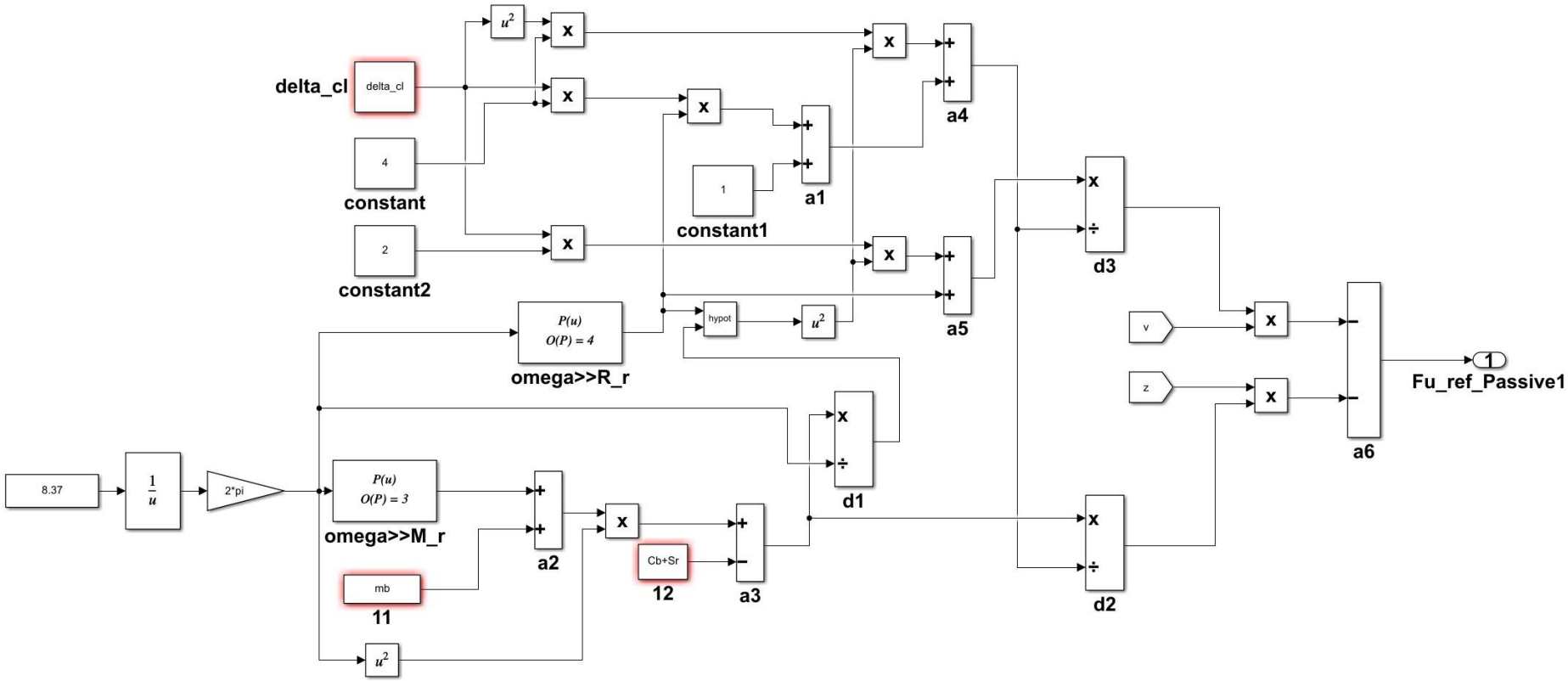

Figure 25: Simulink block for Reactive Control

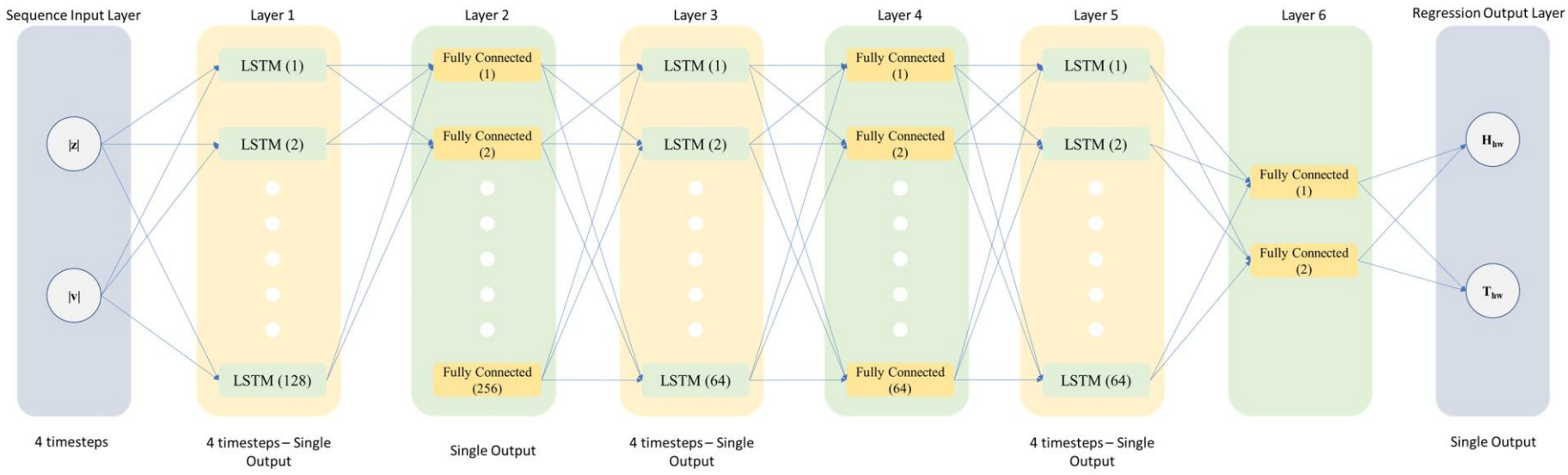

Figure 26: Chosen RNN Architecture

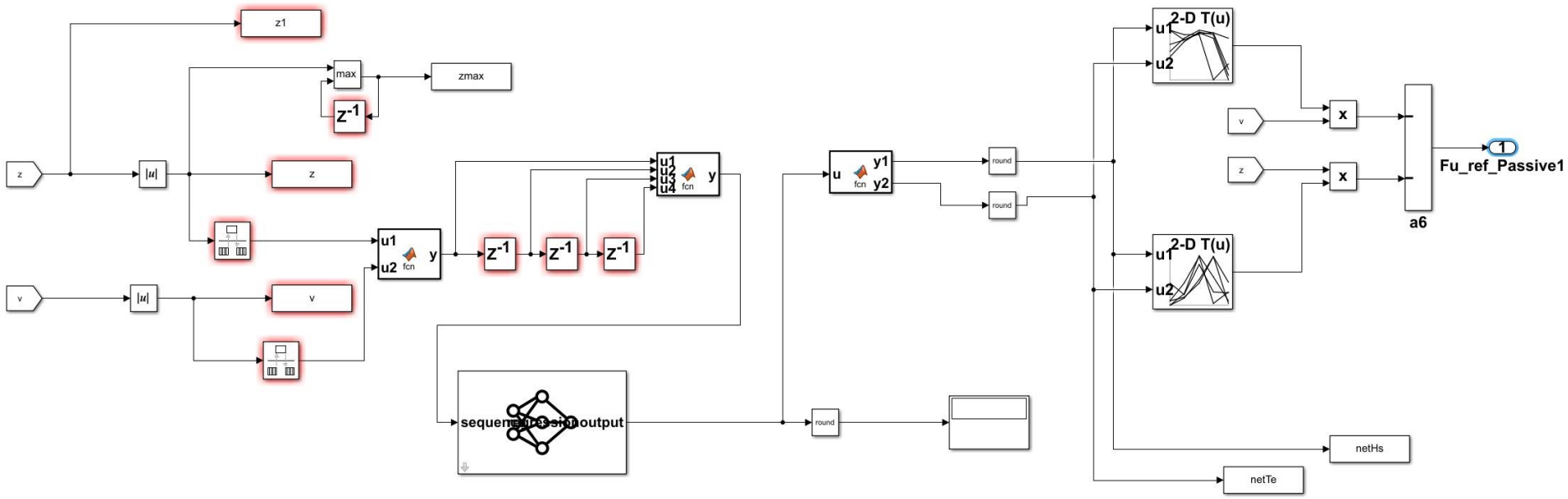

Figure 27: Fully neural network based controller-Simulink

Chapter 3: Results and Discussion

This chapter will discuss the results of the previous sections mentioned in the methodology section. Initially the simulation environment is described based on the initiation parameters. After that, the performance of the Sea State Estimations RNNs is evaluated. Finally, a comparison between the fully neural network based Reactive Control is conducted against traditional Reactive Control and Resistive Control.

3.1 Simulation Environment

The simulation for all the previous section has been set up and are shown in Table 1 and the run times for the simulation of each section is shown in Table 2.

Table 1: Simulation Parameters

Parameter	Value
C_b	1.9737
S_r	6×10^4
C_d	0
λ_{pm}	20 Wb
p_w	0.045 m
R_s	2 Ω
L_s	25×10^{-3}H
Ψ_{pm}	19.8 Wb
draft	1.5 m
Maximum F_u	1.5 N
Range R_{pto}	0 to 4
Range K_{PTO}	0 to -2
Maximum displacement	2 m
Natural frequency	0.75 rad/s

Table 2: Simulation Runtimes

Section	Time per iteration
Sea State Estimation (training & results)	200 s
RC using ANN (training)	1000 s
RC using ANN (Results)	500 s
Wave Sequence	1000 s

Force modelling, equations and state space representations are found by using MATLAB to implement the methodology section. The Simulink simulation runs after. The Sea states used for training and testing are summarized in Table 3.

Table 3: Sea States

#	1 to 3	4-6	7-9	10
H_{hw}(m)	1	2	7-9	2
T_{hw}(s)	8 to 10	8 to 10	8 to 10	8
State	Regular	Regular	Regular	Irregular

The first 9 states are used to train the neural network models in both cases which are sea state estimation and control optimization. The final sea state, which is irregular, is used to evaluate the performance in irregular sea states.

3.2 Simulation Results

3.2.1 Reactive control using neural networks

The optimization algorithm was run multiple times to optimize the damping and stiffness coefficients, These coefficients are listed in Tables 4 and 5.

Table 4: Optimized damping coefficients $\times 10^5$

	1	2	3	4	5
8	1.96	3.1	3.8622	3.6631	0.5635
9	2.3306	3.3930	3.9865	3.7575	3.3989
10	2.8693	3.2309	3.6816	3.7575	1.0192
11	4	3.6608	3.6094	0.1983	1.4044
12	4	3.2404	3.7575	3.3989	0.1983

Table 5: Optimized stiffness coefficients $\times -10^5$

	1	2	3	4	5
8	2	1.55	0.005103	0.8837	1.8104
9	2	1.712	1.0093	0.0087167	1.9278
10	1.8133	1.6798	1.1321	0.0087167	1.0825
11	1.1488	1.5729	0.4204	1.4620	1.5021
12	1.8103	1.1332	0.0872	1.9278	1.4620

All the values lie within the maximum and minimum range of damping (0 to 4×10^5) and stiffness (-2×10^5 to 0) set in the algorithm settings. In order to evaluate the performance, the average electrical power and maximum displacement are placed in comparison to traditional reactive control. This is to ensure that the algorithm is maximizing power while maintaining the constraints. This comparison is illustrated in Table 6. Traditional reactive control is as described in equations 2.29 to 2.34:

Table 6: Traditional vs Optimized Reactive Control Outputs. Power $\times 10^4$ (W), Displacement (m)

H_{hw} , T_{hw}	Optimized max z	Traditional max z	Optimized Power	Traditional Power
1 , 8	1.3580	1.6977	3.4224	2.0755
1 , 9	1.3489	1.6618	2.9225	2.055
1 , 10	1.2295	1.5851	2.6272	1.9878
2 , 8	1.9142	2.7015	8.2588	3.3576
2 , 9	1.9394	2.7280	6.8684	3.9509
2 , 10	2.0570	2.6746	5.9530	4.4386
3 , 8	2.0255	3.6617	13.492	4.4703
3 , 9	2.3300	3.7151	13.303	6.0265
3 , 10	2.5238	3.6728	9.8697	7.5196

It can be observed that the power output has improved in all cases, however for the last two cases the displacement constraint has been violated. This can be resorted to poor neural network prediction on edge cases, or simply because of the behavior of the device during sea states significantly higher than the device size. By intuition, larger displacement should lead to higher power absorption. However, displacement does not solely contribute to the control force as mentioned in Equation 2.29. A better metric is to measure the mechanical power, electrical power and the efficiency as described in Equation 2.49,

Equation 2.51 and Equation 2.52. The power generation and efficiency were compared between both types of control for a regular sea state of $H_{hw} = 3\ m$ & $T_{hw} = 10\ s$:

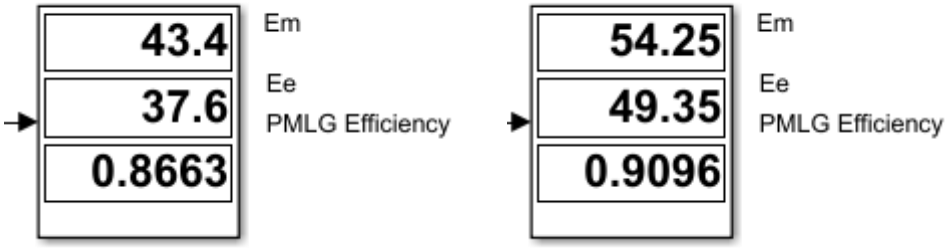

(a) Traditional reactive control (b) Optimized reactive control

Figure 28: Mechanical power, electrical power and efficiency for a regular sea state of H_{hw} =3 m & T_{hw} =10 s. a) Traditional reactive control b) Optimized reactive control

In the case of optimized control, the output mechanical and electrical power are improved as well as the efficiency. The conclusion here is that the optimization improves the power output and efficiency during all sea states. However, the displacement constraint is not maintained in all sea states.

3.2.2 Sea state estimation using recurrent neural networks

The RNNs developed are evaluated based on training time and Root Mean Square Error (RMSE). Networks that have a lower RMSE are considered higher in performance. Training time is important for online applications where quicker training is required.

However, the case in this work is done offline, but it matters to portray the capability of certain architectures to learn the non-linear relationships between input and output faster. The training graphs exported from MATLAB for both GRU and LSTM are shown in Figure 29 and Figure 30. For both cases, the batch size was chosen 128. Training time is similar in both cases however the RMSE for LSTM is lower. This is a clear indicator that the main network used for estimation should be the LSTM network. Another outcome to be deduced is that LSTM is better at handling time series data for this application, as in its more suitable in solving the vanishing gradient problem. Intuitively, GRU should take less time to complete the training. mainly resorted to the presence of less gates which means less processing time. This is confirmed in [57]. However, this was not

the case in this application. Additionally, the performance of the LSTM network might be better since the extra processing per memory cell is better at handling this specific problem.

Following the choice of LSTM, the network had to be tested under different H_{hw} and T_{hw} to check the capability of homing into the correct sea state eventually. To do that, the output of the RNN is collected after being connected in the complete controller. The performance for multiple regular sea states is shown in Figure 31 and Figure 32. Overall, the prediction stabilizes after 50 seconds of simulation, this is due to the dynamics stabilizing after this period. The model performs well in sea states with higher periods, whereas the prediction fluctuates in lower periods. This can be resorted to the algorithm not being fast enough for the lower wave periods.

Additionally, the model was used with the optimized look up tables to control the irregular sea state from Table 3, this is then compared with the performance in traditional reactive control. This is shown in Figure 33. It is easy to observe that the NN based reactive control maintained the displacement constraints in the irregular wave and also yields higher power output. Finally, the model is tested in a sequence of regular waves. This consisted of 5 waves each lasting 200 s. The sequence in half wave height and period respectively is (1-9), (1-10), (2-9), (2-10) and (3-9). The results are shown in Figure 34. As observed from the Figure, the neural network model is working as intended with the exception of the 50-60 s required for the dynamics to settle between waves. However, quick fluctuations in the third sea state can be observed. A solution to this problem can be increasing the model's accuracy. This is further discussed in the recommendations section.

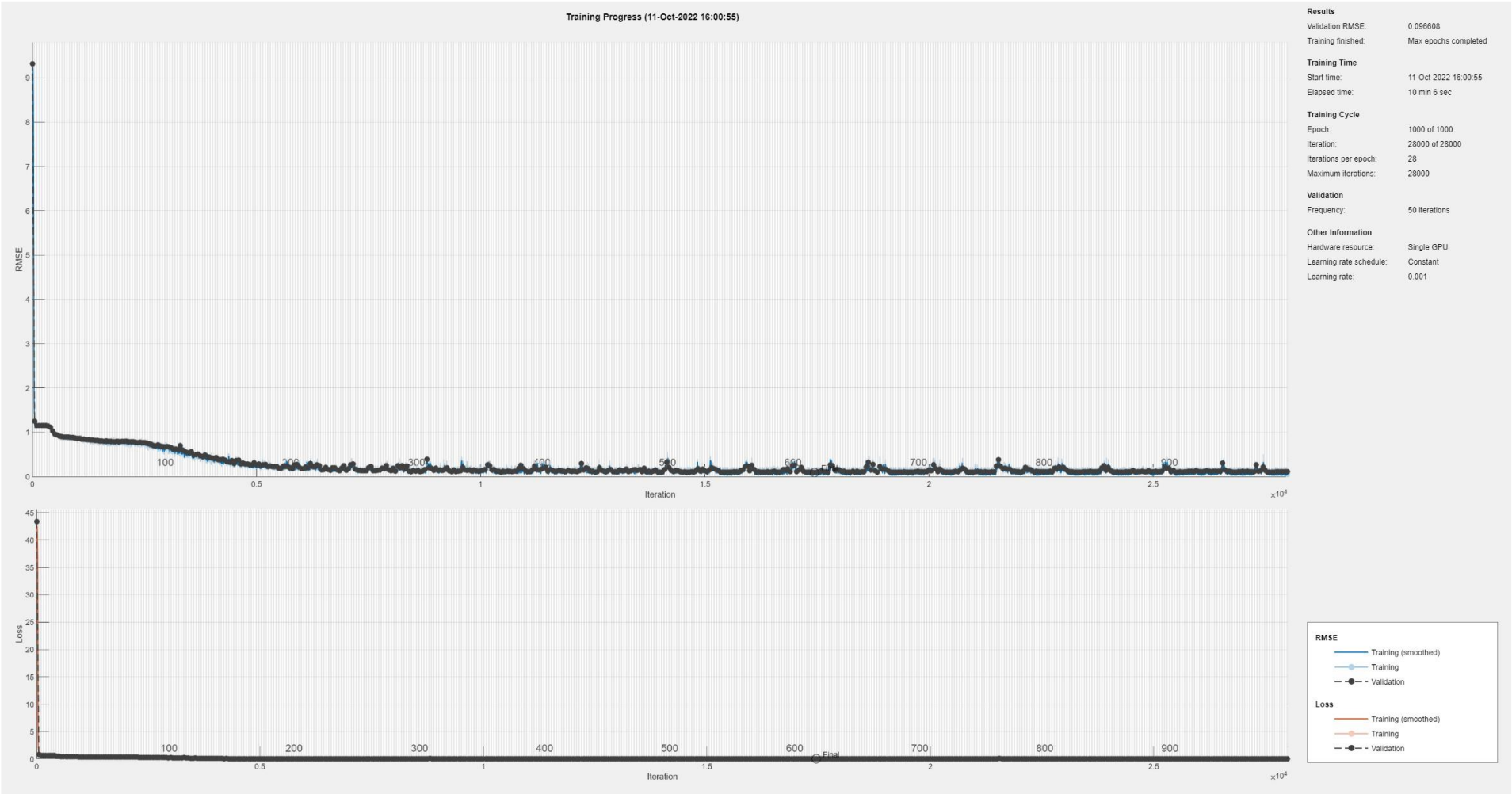

Figure 29: Training graph for LSTM

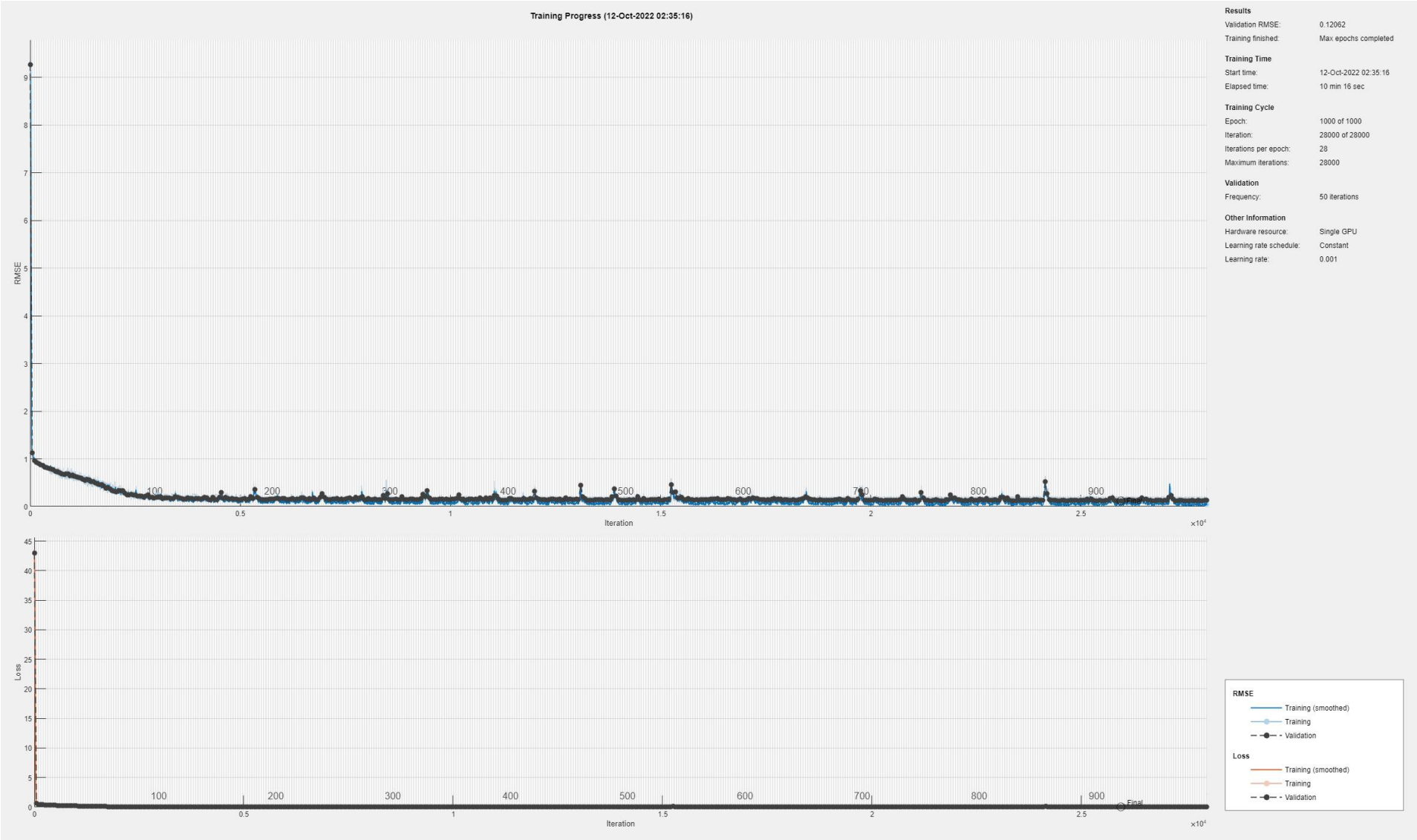

Figure 30: Training progress graphs for RNNs

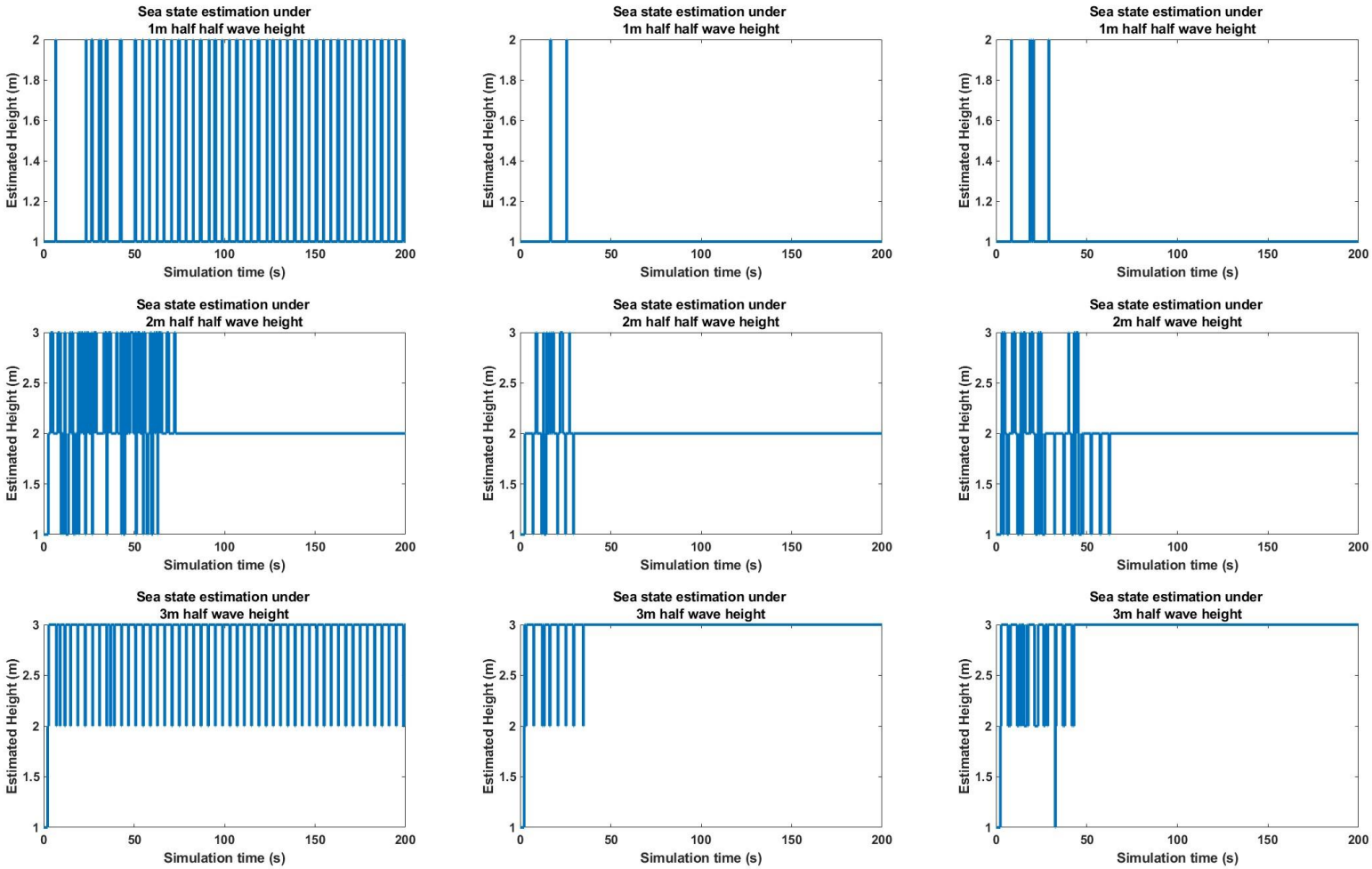

Figure 31: Prediction results for half wave height

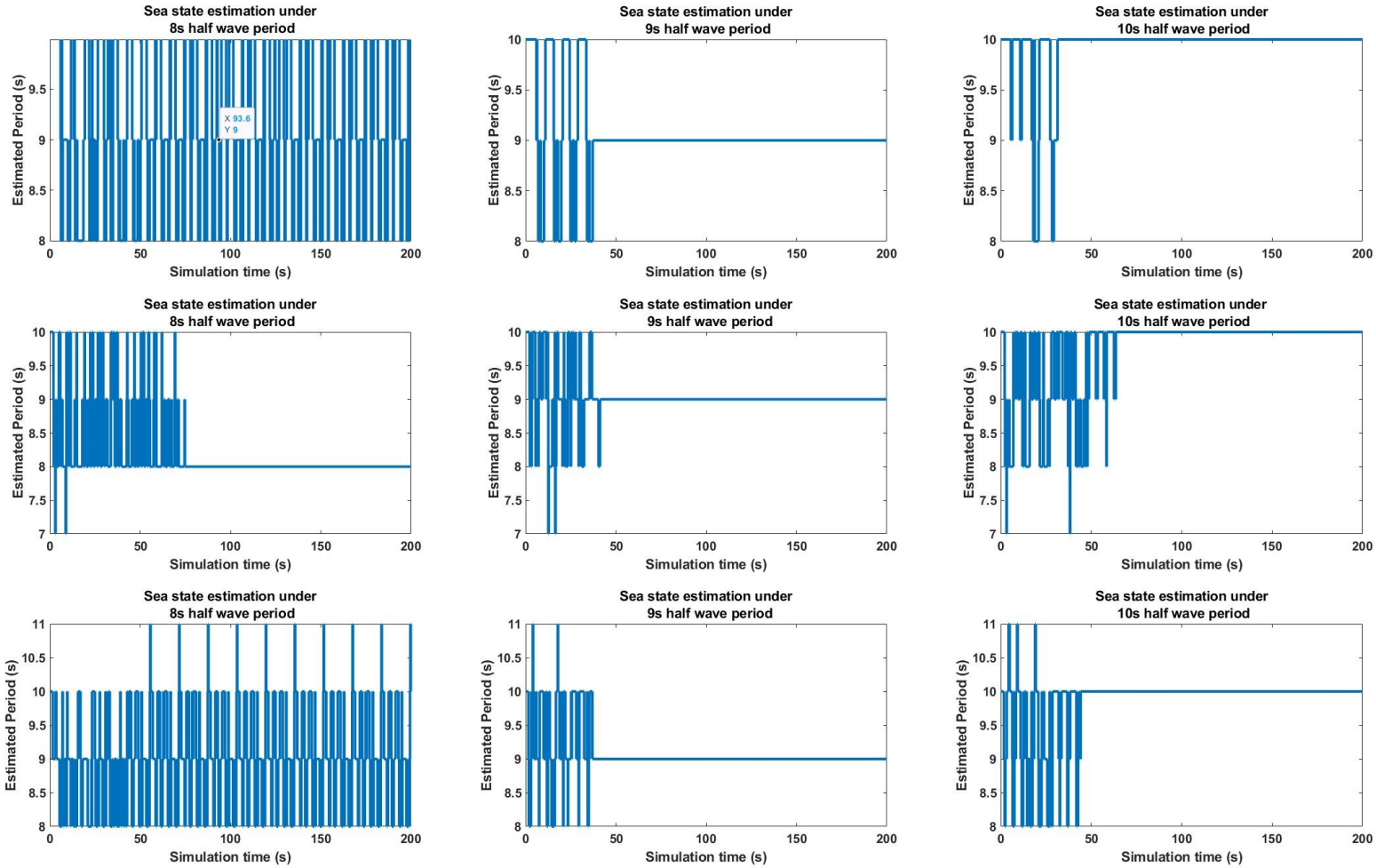

Figure 32: Prediction results for half wave period

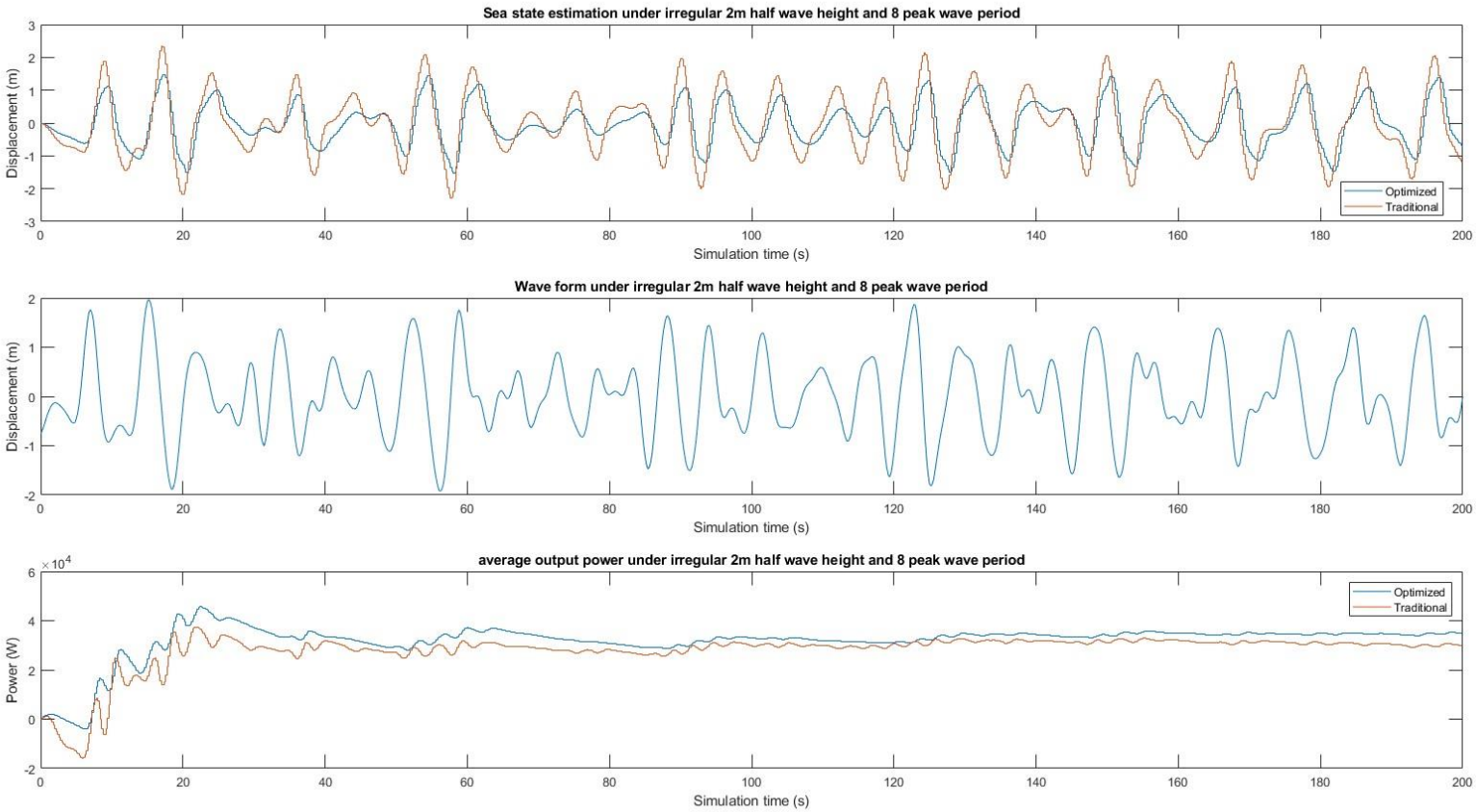

Figure 33: Prediction results for irregular waves

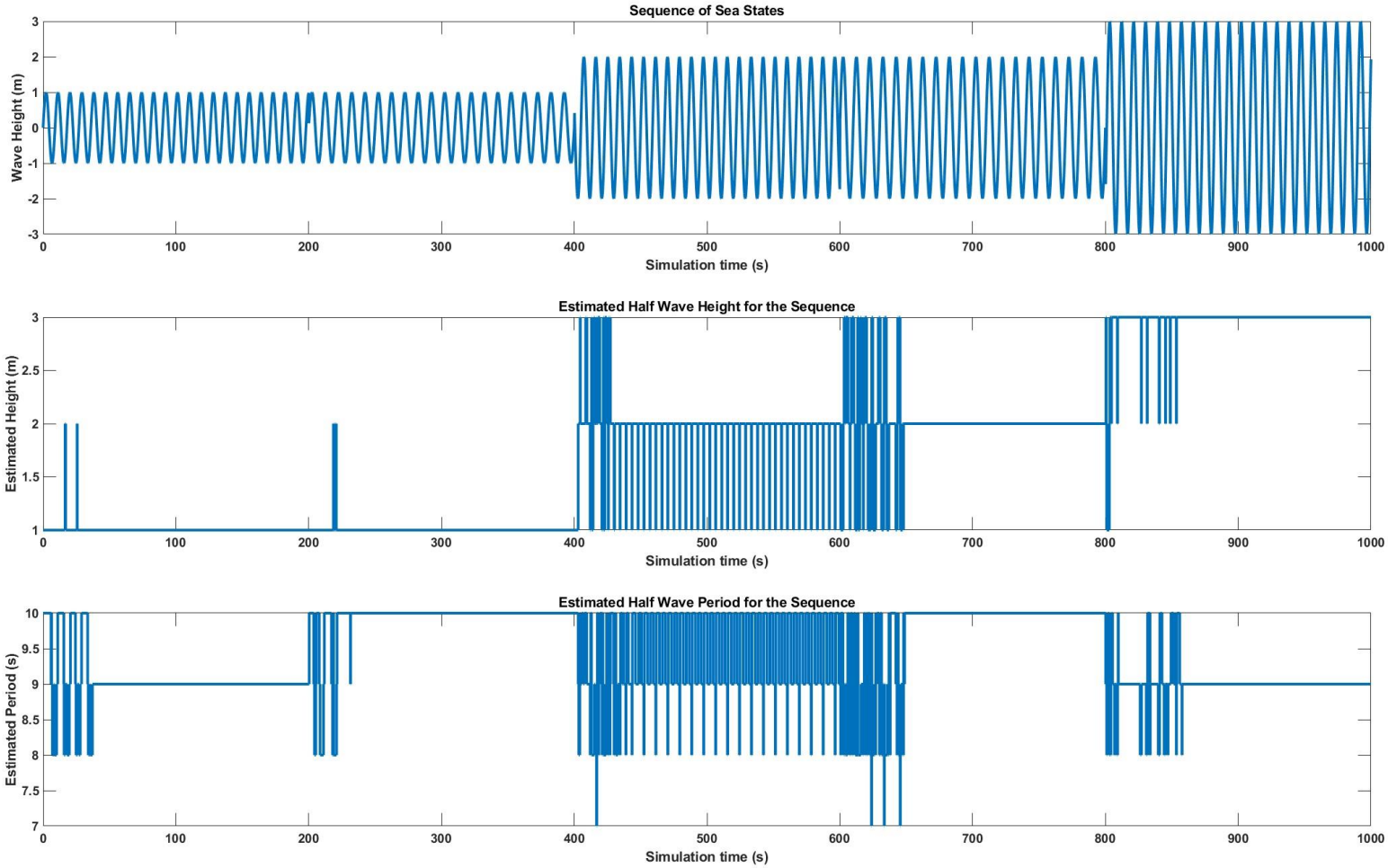

Figure 34: Prediction results for sequence of regular waves

Chapter 4: Conclusion

In this Master's thesis, a neural network based reactive control technique is proposed for wave energy converters. The power take-off forces and electromagnetic force are the main contributor to maximizing the power output in reactive control. An average model of the WEC is simulated as a basis for assessment of the neural network algorithms. The main objectives are improving reactive control using existing neural network research, estimating the sea state in real time and creating a controller that is fully based on these networks.

4.1 Research Findings & Summary

The main findings and contributions are highlighted below:

- Optimizing the power output of reactive control using feed forward neural networks and global optimization to improve the power output. This is done through exploration of random damping and stiffness coefficients within a defined search space and training neural networks as the cost functions of the minimization algorithm. All this is done while maintaining the displacement constraints of the WEC. The optimized coefficients are used to create look up tables.
- Proposed a method of estimating sea states in real time. This is done through the creating recurrent neural network architectures, evaluating them and deploying to give real time measurements of the sea state.
- Creating a controller that is based on sea state output from the RNNs feeding into the look up tables to find the optimal damping and stiffness coefficients. Consequently, this leads to outputting the reference control force needed.

4.2 Limitations

The limitations of the current work are:

- Training of the neural networks was done on a limited number of sea states and intervals.
- Evaluation of performance in irregular waves was only measured by average power. There is not a method yet to evaluate individual peaks/troughs.

- The current RNN RMSE needs improvement, and real-time fluctuations need to be dealt with better.
- Faster waves experience more fluctuations in prediction.

4.3 Future Work

The areas of improvement that can add to the contribution of this thesis are:

- Experimenting with more datasets. Identifying inputs that can help the RNN learn the non-linear relationship between inputs and outputs can be very crucial to its performance.
- Making the RNN capable of making faster predictions. By using shorter time steps in the time series data, the network should be able to perform better in lower wave periods.
- Identifying performance decay parameters in long term deployment of the WEC. This can lead to the implementation of a continuous learning pipeline that can adapt to the changes the WEC faces in real life due to corrosion and marine life growth.
- Implementing methods of measuring displacement and velocity. Currently, the assumption of the presence of these measurements is made. However, by finding a solution to this problem a standalone system can be deployed without the need for expensive measuring instruments.
- Applying the developed technique to hardware experiments.
- Creating a more efficient architecture for the RNN. A more efficient (deeper or wider) architecture should be capable of learning more features which leads to lower RMSE. This can also mean the possibility of handling bigger datasets.

References

[1] V. Smil, *Energy Transitions: Global and National Perspectives*, 2nd Edition. Dec. 2016.

[2] "Bp Statistical Review of World Energy," Tech. Rep., 2022. [Online]. Available: https://www.bp.com/content/dam/bp/businesssites/en/global/corporate/pdfs/energy-economics/ statistical-review/bp-stats-review-2022-full-report.pdf (visited on 08/21/2022).

[3] UAE Energy Diversification | UAE Embassy in Washington, DC, en. [Online]. Available: https://www.uae-embassy.org/discover-uae/climate-and-energy/uae-energy-diversification(visited on 08/22/2022).

[4] H. Ritchie and M. Roser, Fossil Fuels. [Online]. Available: https://ourworldindata.org/fossilfuels (visited on 08/21/2022).

[5] Renewable Energy. [Online]. Available: https://www.c2es.org/content/renewable-energy/(visited on 08/22/2022).

[6] J. Cruz, Ed., Ocean wave energy: current status and future prepectives [i.e. perspectives] (Green energy and technology). Berlin: Springer, 2008, OCLC: ocn181069659, ISBN: 978-3-540-74894-6.

[7] M. E. McCormick, Ocean engineering mechanics: with applications. Cambridge ; New York: Cambridge University Press, 2010, OCLC: ocn318672282, ISBN: 978-0-521-85952-3.

[8] J. Falnes, Ocean waves and oscillating systems: linear interactions including wave-energy extraction. Cambridge ; New York: Cambridge University Press, 2002, ISBN: 978-0-521-78211-1.

[9] F. Fusco and J. V. Ringwood, "A Simple and Effective Real-Time Controller for Wave Energy Converters," IEEE Transactions on Sustainable Energy, vol. 4, no. 1, pp. 21–30, Jan. 2013, ISSN: 1949-3029, 1949-3037. DOI: 10.1109/TSTE.2012.2196717. [Online]. Available: http://ieeexplore.ieee.org/ document/6205353/ (visited on 08/23/2022).

[10] N. O. a. A. A. US Department of Commerce, Corals: NOAA's National Ocean Service Education, EN-US.[Online]. Available: https://oceanservice.noaa.gov/education/tutorial_currents/media/supp_cur03a.html (visited on 08/23/2022).

[11] S. J. Russell and P. Norvig, Artificial intelligence: a modern approach (Pearson Series in Artificial Intelligence), eng, Fourth edition, global edition. Harlow: Pearson, 2022, ISBN: 978-1-292-40113-3.

[12] Simplifying the Difference: Machine Learning vs Deep Learning - Singapore Computer Society. url: Https://www.scs.org.sg/artic learning-vs-deep-learning. [Online]. Available: https://www.scs.org.sg/articles/machinelearning-vs-deep-learning (visited on 08/28/2022).

[13] W. S. McCulloch and W. Pitts, "A logical calculus of the ideas immanent in nervous activity," en, Bulletin of Mathematical Biology, vol. 52, no. 1-2, pp. 99–115, Jan. 1990, ISSN: 0092-8240, 1522-9602. DOI: 10.1007/ BF02459570. [Online]. Available: http://link.springer.com/10.1007/BF02459570 (visited on 08/28/2022).

[14] Kaggle: Your Machine Learning and Data Science Community, en. [Online]. Available: https://www. kaggle.com/ (visited on 11/14/2022).

[15] I. J. Goodfellow, J. Pouget-Abadie, M. Mirza, et al., Generative Adversarial Networks, arXiv:1406.2661 [cs, stat], Jun. 2014. [Online]. Available: http://arxiv.org/abs/1406.2661 (visited on 10/12/2022).

[16] E. Anderlini, D. Forehand, E. Bannon, and M. Abusara, "Reactive control of a wave energy converter using artificial neural networks," en, International Journal of Marine Energy, vol. 19, pp. 207–220, Sep. 2017, ISSN: 22141669. DOI: 10.1016/j.ijome.2017.08.001. [Online]. Available: https://linkinghub. elsevier.com/retrieve/pii/S2214166917300668 (visited on 08/28/2022).

[17] E. Anderlini, D. I. M. Forehand, P. Stansell, Q. Xiao, and M. Abusara, "Control of a Point Absorber Using Reinforcement Learning," IEEE Transactions on Sustainable Energy, vol. 7, no. 4, pp. 1681–1690, Oct. 2016, ISSN: 1949-3029, 1949-3037. DOI: 10.1109/TSTE.2016.2568754. [Online]. Available: https: //ieeexplore.ieee.org/document/7482650/ (visited on 08/28/2022).

[18] F. Pierart, C. Manriquez, and P. Campos, "Reinforcement learning algorithms applied to reactive and resistive control of a wave energy converter," in 2021 IEEE CHILEAN Conference on Electrical, Electronics Engineering, Information and Communication Technologies (CHILECON), Valparaíso, Chile: IEEE, Dec. 2021, pp. 1– 6, ISBN: 978-1-66540-873-8. DOI:10.1109/CHILECON54041.2021.9702963. [Online]. Available: https://ieeexplore.ieee.org/document/9702963/ (visited on 08/28/2022).

[19] O. Abdelkhalik and H. Abdulkadir, “Optimal Control of Wave Energy Converters,” in OCEANS 2021: San Diego – Porto, San Diego, CA, USA: IEEE, Sep. 2021, pp. 1–5, ISBN: 978-0-692-93559-0. DOI: 10.23919/OCEANS44145.2021.9705961. [Online]. Available: https://ieeexplore.ieee.org/document/ 9705961/ (visited on 08/28/2022).

[20] E. S. J. Hesam, B. Ling, and B. A. Batten, “Use of artificial neural networks for real-time prediction of heave displacement in ocean buoys,” in 2014 International Conference on Renewable Energy Research and Application (ICRERA), Milwaukee, WI, USA: IEEE, Oct. 2014, pp. 907–912, ISBN: 978-1-4799-3795-0. DOI:10.1109/ICRERA.2014.7016517. [Online]. Available: http://ieeexplore.ieee.org/ document/7016517/ (visited on 08/28/2022).

[21] M. Jama, A. Wahyudie, and S. Mekhilef, “Wave Excitation Force Estimation Using an Electrical-Based Extended Kalman Filter for Point Absorber Wave Energy Converters,” IEEE Access, vol. 8, pp. 49823–49836, 2020, ISSN: 2169-3536. DOI: 10.1109/ACCESS.2020.2980229. [Online]. Available: https://ieeexplore.ieee.org/document/9034016/ (visited on 08/28/2022).

[22] M. Jama, “CONTROL STRATEGIES FOR IMPROVING THE PERFORMANCE OF HEAVING WAVE ENERGY CONVERTERS,” Ph.D. dissertation, United Arab Emirates University, Al Ain, Abu Dhabi, UAE, Jun. 2015.

[23] A. de la Villa Jaén, A. García-Santana, and D. E. Montoya-Andrade, “Maximizing output power of linear generators for wave energy conversion: Maximizing power of linear generators for WEC,” en, International Transactions on Electrical Energy Systems, vol. 24, no. 6, pp. 875–890, Jun. 2014, ISSN: 20507038. DOI: 10.1002/etep.1747. [Online]. Available: https://onlinelibrary.wiley.com/doi/10. 1002/etep.1747 (visited on 09/03/2022).

[24] E. Konstantinidis, J. Zhao, J. Leontini, D. Lo Jacono, and J. Sheridan, “Excitation and Damping Fluid Forces on a Cylinder Undergoing Vortex-Induced Vibration,” Frontiers in Physics, vol. 7, p. 185, Nov. 2019, ISSN: 2296-424X. DOI: 10.3389/fphy.2019.00185. [Online]. Available: https://www.frontiersin. org/article/10.3389/fphy.2019.00185/full (visited on 09/04/2022).

[25] R. Taghipour, T. Perez, and T. Moan, “Hybrid frequency–time domain models for dynamic response analysis of marine structures,” en, Ocean Engineering, vol. 35, no. 7, pp. 685–705, May 2008, ISSN: 00298018. DOI:10.1016/j.oceaneng.2007.11.002. [Online]. Available: https://linkinghub.elsevier. com/retrieve/pii/S0029801807002363 (visited on 09/03/2022).

[26] A. McCabe, T. Stallard, N. Baker, and H. Yavuz, “Estimation of the responses of axisymmetric bodies in spread irregular waves,” en, Ocean Engineering, vol. 34, no. 10, pp. 1371–1382, Jul. 2007, ISSN: 00298018. DOI:10.1016/j.oceaneng.2006.10.004. [Online]. Available: https://linkinghub.elsevier. com/retrieve/pii/S0029801806002411 (visited on 09/04/2022).

[27] T. Perez and T. I. Fossen, “Practical aspects of frequency-domain identification of dynamic models of marine structures from hydrodynamic data,” en, Ocean Engineering, vol. 38, no. 2-3, pp. 426–435, Feb. 2011, ISSN: 00298018. DOI: 10.1016/j.oceaneng.2010.11.004. [Online]. Available: https:// linkinghub.elsevier.com/retrieve/pii/S0029801810002490 (visited on 09/04/2022).

[28] J. Falnes, “Principles for capture of energy from ocean waves. Phase control and optimum oscillation.,” 1976. [Online]. Available: https://citeseerx.ist.psu.edu/viewdoc/summary?doi=10.1.1. 184.7996.

[29] M. S. Forsthoffer, “Compressors,” en, in Forsthoffer’s More Best Practices for Rotating Equipment, Elsevier, 2017, pp. 73–185, ISBN: 978-0-12-809277-4. DOI: 10.1016/B978-0-12-809277-4.00003-6. [Online]. Available: https://linkinghub.elsevier.com/retrieve/pii/B9780128092774000036(visited on 09/13/2022).

[30] M. Eriksson, Modelling and experimental verification of direct drive wave energy conversion: buoy-generator dynamics, eng. Uppsala: Acta Universitatis Upsaliensis Acta Universitatis Upsaliensis, 2007, OCLC: 938423643, ISBN: 978-91-554-6850-7.

[31] O. Danielsson, Wave energy conversion: linear synchronous permanent magnet generator, eng. Uppsala: Acta Universitatis Upsaliensis, 2006, OCLC: 185426059, ISBN: 978-91-554-6683-1.

[32] Z. Ballard and B. P. Mann, “Two-Dimensional Nonlinear Analysis of an Untethered Spherical Buoy Due to Wave Loading,” en, Journal of Computational and Nonlinear Dynamics, vol. 8, no. 4, p. 041019, Oct. 2013, ISSN: 1555-1415, 1555-1423. DOI: 10.1115/1.4024887. [Online]. Available: https://asmedigitalcollection.asme.org/computationalnonlinear/article/doi/10.1115/1.4024887/370797/ TwoDimensional-Nonlinear-Analysis-of-an-Untethered (visited on 09/06/2022).

[33] B. Wade and M. Dwyer, “Application of Morison’s Equation to Fixed Offshore Platforms,” en, Journal of Petroleum Technology, vol. 30, no. 03, pp. 447–454, Mar. 1978, ISSN: 0149-2136, 1944-978X. DOI: 10.2118/6324-PA. [Online]. Available: https://onepetro.org/JPT/article/30/03/447/ 168044/Application-of-Morison-s-Equation-to-Fixed (visited on 09/06/2022).

[34] M. Bhinder, A. Babarit, L. Gentaz, and P. Ferrant, “Effect of Viscous Forces on the Performance of a Surging Wave Energy Converter,” 193644 Bytes, 2015, Artwork Size: 193644 Bytes Publisher: figshare. DOI: 10.6084/M9.FIGSHARE.1418017. [Online]. Available: https://figshare.com/articles/journal_contribution/Effect_of_Viscous_Forces_on_the_Performance_of_a_Surging_Wave_Energy_Converter/1418017 (visited on 09/06/2022).

[35] M. Leijon, O. Danielsson, M. Eriksson, et al., “An electrical approach to wave energy conversion,” en, Renewable Energy, vol. 31, no. 9, pp. 1309–1319, Jul. 2006, ISSN: 09601481. DOI: 10.1016/j.renene.2005.07.009. [Online]. Available: https://linkinghub.elsevier.com/retrieve/pii/ S0960148105002120 (visited on 09/06/2022).

[36] A. Price, “New Perspectives on Wave Energy Converter Control,” Ph.D. dissertation, The University of Edinburgh, Mar. 2009.

[37] W. Cummins, “The impulse resonse function and ship motions,” Institut flir Schiffbau der Universitit Hamburg, Tech. Rep., 1962.

[38] R. Alcorn, D. O’Sullivan, and I. of Engineering and Technology, Eds., Electrical design for ocean wave and tidal energy systems (IET renewable energy series 17). Stevenage, U.K: Institution of Engineering and Technology, 2013, OCLC: ocn874844781, ISBN: 978-1-84919-561-4.

[39] I. Boldea and S. A. Nasar, Linear electric actuators and generators. Cambridge ; New York: Cambridge University Press, 1997, ISBN: 978-0-521-48017-8.

[40] H. Abu-Rub, A. Iqbal, and J. Guzinski, High performance control of AC drives with MATLAB/Simulink models. Chichester, West Sussex ; Hoboken, NJ: Wiley, 2012, ISBN: 978-0-470-97829-0.

[41] J. C. Alacoque, Direct eigen control for induction machines and synchronous motors. [Piscataway, N.J.?] : Chichester, West Sussex, United Kingdom: IEEE Press ; Wiley, 2013, ISBN: 978-1-119-94270-2.

[42] A. de la Villa Jaén, D. E. M. Andrade, and A. García Santana, “Increasing the efficiency of the passive loading strategy for wave energy conversion,” en, Journal of Renewable and Sustainable Energy, vol. 5, no. 5, p. 053132, Sep. 2013, ISSN: 1941-7012. DOI: 10.1063/1.4824416. [Online]. Available: http://aip.scitation.org/doi/10.1063/1.4824416 (visited on 09/13/2022).

[43] L. Wang, PID and predictive control of electrical drives and power converters using MATLAB/Simulink. Solaris South Tower, Singapore: IEEE, Wiley, 2015, ISBN: 978-1-118-33944-2.

[44] M. Chinchilla, S. Arnaltes, and J. Burgos, “Control of Permanent-Magnet Generators Applied to VariableSpeed Wind-Energy Systems Connected to the Grid,” en, IEEE Transactions on Energy Conversion, vol. 21, no. 1, pp. 130–135, Mar. 2006, ISSN: 0885-8969. DOI: 10.1109/TEC.2005.853735. [Online]. Available: http://ieeexplore.ieee.org/document/1597329/ (visited on 09/26/2022).

[45] R. Kalman, “A New Approach to Linear Filtering and Prediction Problems,” pp. 35–45, 1960.

[46] A. Tealab, “Time series forecasting using artificial neural networks methodologies: A systematic review,” en, Future Computing and Informatics Journal, vol. 3, no. 2, pp. 334–340, Dec. 2018, ISSN: 23147288. DOI:10.1016/j.fcij.2018.10.003. [Online]. Available: https://linkinghub.elsevier.com/retrieve/pii/S2314728817300715 (visited on 09/27/2022).

[47] N. Yadaiah and G. Sowmya, “Neural Network Based State Estimation of Dynamical Systems,” in The 2006 IEEE International Joint Conference on Neural Network Proceedings, Vancouver, BC, Canada: IEEE, 2006, pp. 1042–1049, ISBN: 978-0-7803-9490-2. DOI: 10.1109/IJCNN.2006.1716214. [Online]. Available: https://ieeexplore.ieee.org/document/1716214 (visited on 09/27/2022).

[48] Y. LeCun, Y. Bengio, and G. Hinton, “Deep learning,” en, Nature, vol. 521, no. 7553, pp. 436–444, May 2015, ISSN: 0028-0836, 1476-4687. DOI: 10.1038/nature14539. [Online]. Available: http://www.nature.com/articles/nature14539 (visited on 09/28/2022).

[49] M. T. Hagan, H. B. Demuth, and M. H. Beale, Neural network design, 1st ed. Boston: PWS Pub, 1996, ISBN: 978-0-534-94332-5.

[50] D. P. Kingma and J. Ba, Adam: A Method for Stochastic Optimization, arXiv:1412.6980 [cs], Jan. 2017. [Online]. Available: http://arxiv.org/abs/1412.6980 (visited on 10/08/2022).

[51] S. Hochreiter and J. Schmidhuber, “Long Short-Term Memory,” en, Neural Computation, vol. 9, no. 8, pp. 1735– 1780, Nov. 1997, ISSN: 0899-7667, 1530-888X. DOI: 10.1162/neco.1997.9.8.1735. [Online]. Available: https://direct.mit.edu/neco/article/9/8/1735-1780/6109 (visited on 09/28/2022).

[52] A. Ng, Long Short Term Memory (LSTM), en. [Online]. Available: https://www.coursera.org/ learn/nlp-sequence-models/lecture/KXoay/long-short-term-memory-lstm (visited on 10/08/2022).

[53] C. Olah, Understanding LSTM Networks – colah’s blog. [Online]. Available: https://colah.github. io/posts/2015-08-Understanding-LSTMs/ (visited on 10/08/2022).

[54] K. Cho, B. van Merrienboer, D. Bahdanau, and Y. Bengio, On the Properties of Neural Machine Translation: Encoder-Decoder Approaches, arXiv:1409.1259 [cs, stat], Oct. 2014. [Online]. Available: http://arxiv. org/abs/1409.1259 (visited on 10/08/2022).

[55] A. Ng, Gated Recurrent Unit (GRU), en. [Online]. Available: https://www.coursera.org/learn/ nlp-sequence-models/lecture/agZiL/gated-recurrent-unit-gru (visited on 10/08/2022).

[56] Z. Ugray, L. Lasdon, J. Plummer, F. Glover, J. Kelly, and R. Martí, “Scatter Search and Local NLP Solvers: A Multistart Framework for Global Optimization,” en, INFORMS Journal on Computing, vol. 19, no. 3, pp. 328– 340, Aug. 2007, ISSN: 1091-9856, 1526-5528. DOI: 10.1287/ijoc.1060.0175. [Online]. Available: http://pubsonline.informs.org/doi/10.1287/ijoc.1060.0175 (visited on 10/08/2022).

[57] S. Yang, X. Yu, and Y. Zhou, “LSTM and GRU Neural Network Performance Comparison Study: Taking Yelp Review Dataset as an Example,” in 2020 International Workshop on Electronic Communication and Artificial Intelligence (IWECAI), Shanghai, China: IEEE, Jun. 2020, pp. 98–101, ISBN: 978-1-72818-149-3. DOI: 10.1109/IWECAI50956.2020.00027. [Online]. Available: https://ieeexplore.ieee. org/document/9221727/ (visited on 10/10/2022).

UAE UNIVERSITY MASTER THESIS NO. 2022:103

This work discusses the development of neural network based reactive control system for wave energy converters. It introduces a novel sea state estimation technique using recurrent neural networks for regular and irregular wave sea state estimation. The sea state estimation technique is used in addition to state of the art neural network based reactive control techniques to optimize the power absorption of point absorber wave energy converters.

Abdelmoamen Ali Nasser received his Master of Science in Electrical Engineering from the Department of Electrical & Communication Engineering, College of Engineering at UAE University, UAE. He received his BSc in Electrical Engineering from the College of Engineering, Abu Dhabi University, UAE.